MSc Thesis in Applied Earth Sciences

Geo-Energy Engineering Track

Fracture characterisation in carbonate reservoirs for geothermal production

Sofia Barreiros Jorge

2022

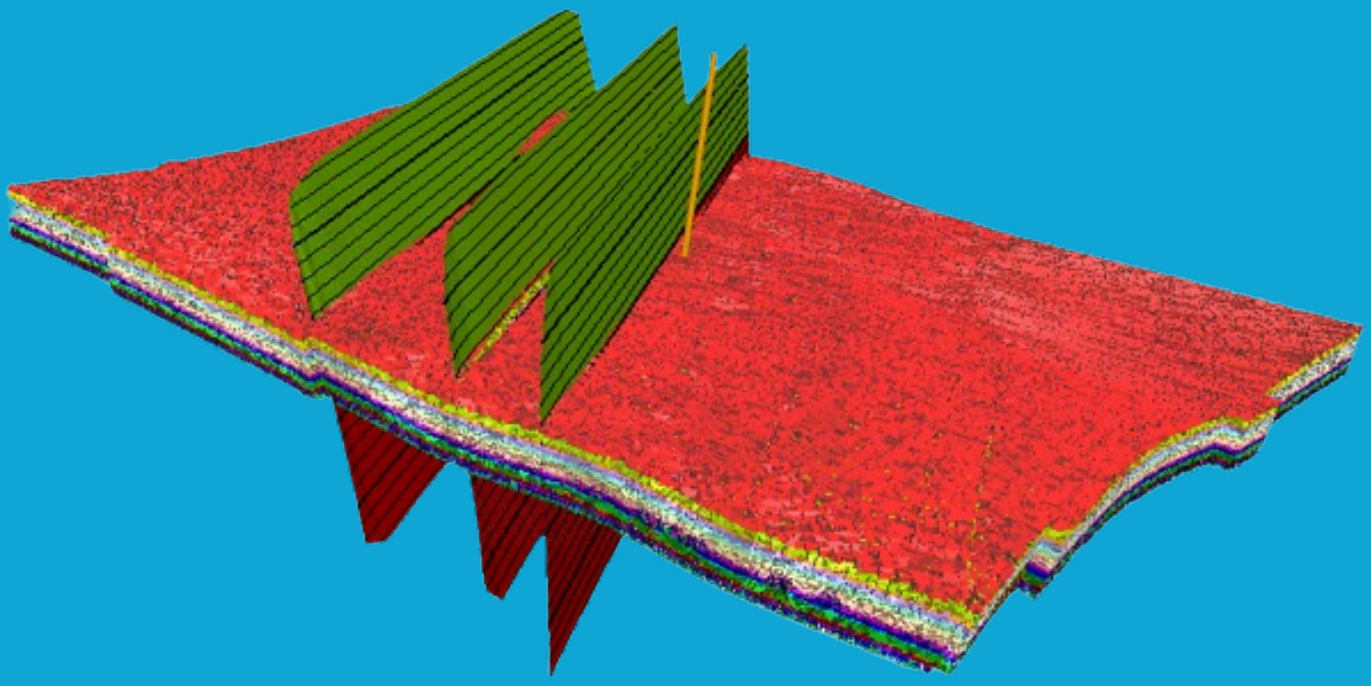

TU Delft

FRACTURE CHARATERISATION IN CARBONATE RESERVOIRS FOR GEOTHERMAL PRODUCTION

A thesis submitted to the Delft University of Technology in partial fulfillment of the requirements for the degree of

Master of Science in Applied Earth Sciences

by

Sofia Barreiros Jorge

August 2022

Supervisors:	Prof.dr. Giovanni Bertotti
	Dr. Pierre-Olivier Bruna
	ir. Prof.dr. David Bruhn
Co-reader:	Dr. Alex Danidillis

ABSTRACT

Subsurface energy projects carry high risk due to the lack of data available to accurately model reservoir characteristics. There is a need for high level analysis to extrapolate subsurface data from a single point (i.e. a well). The focus of this study will be on fracture characterisation in a carbonate reservoir located within the Geneva Basin for the purposes of geothermal exploration. The goal is to use fracture characterisation techniques in the form of an OBI analysis and the use of a fracture growth model with a focus on geomechanics to predict the possible fracture growth patterns. This work will allow for a better understanding of fluid flow and permeability throughout the reservoir. As well as explore the benefits and limitations of this approach. The case study is a fractured carbonate reservoir made up of limestone and marlstone packages. To calculate the paleo stress environment, the fracture data is used to back calculate the possible magnitude of the stress field during fracture formation. This choice was made after careful consideration and comparison of the fracture data with the fault data. The output of this modelling will be a DFN with multiple layers controlled by the fracture density. This model can hopefully be used in the future for dynamic simulation to understand the impacts of these assumptions and validate with production data from the well.

ACKNOWLEDGEMENTS

Before presenting my work I would like to thank my thesis supervisor Pierre Olivier-Bruna who has been incredibly patient and understanding of my way or working. I don't think that I would have had the courage or motivation to finish my degree without the friendly encouragement that he gave me throughout our many meetings and check-ins. From the beginning Pierre has always had my back, making sure that I don't fall down the rabbit hole of scientific research. I really would not have been able to make it close to where I am now without his support. I would also like to thank Michael Welch from DTU who has also provided a lot of support regarding the Discrete Fracture Network generator that I have used in this work too create a model of the fractures in the Reservoir.

I would like to thank Andrea Moscariello from UNIGE who has contributed the data which I have analysed in this work and been very open about discussions related to the case study. I would also like to mention the three other master students which I have collaborated with; Mahmood Alhammad, Myrthe Doesburg, Morgane Koumrouyane, and Kristy Lo who have also spent hours looking at the same fracture data as I have. I admire and have learnt a lot through their analysis.

I really enjoyed being part of this very large team of collaborators surrounding this one particular set of data from the Geneva Basin. During this process I was able to meet and speak to people from three different technical universities exchanging ideas and thoughts. I really enjoyed being a part of something bigger through data. I hope that this data continues to fuel many more research projects to come. I am very much looking forward to what this site will look like within the coming five to ten years.

I would also like to thank Giovanni Bertotti who has also always helped in guiding me through my presentation and giving me pointers on what kind of things I can improve on, his feedback is very much appreciated. Even though our collaboration was short, I would also like to thank Alex Daniilidis for his time explaining the dynamic modelling work flows and hope that someone can take this data to the next step in the following years. I'd like to thank David Bruhn who was there in the early stages who also had a lot of patience and great advice on scope and management.

I would also like to thank my friends for being understanding and patient with me during this whole process. I appreciate that none of them made me feel as though I was not capable of finishing but instead gave me what I needed to continue to follow through with this degree. I really appreciate all of their support. This was definitely a learning process for me, not only about fracture analysis, but also towards how I am as a person and what I can improve upon in my academic and work relationships. I hope that following this thesis project I can learn to be more reliable and manage my time more efficiently.

CONTENTS

LIST OF FIGURES

LIST OF TABLES

1 INTRODUCTION

As the energy demand increases and the urgency for finding alternative solutions to electricity and heating become imminent, there is a socio-political push to diversify the energy supply to become less reliant on fossil fuels. A sustainable and feasible option for supplying a large part of the heating energy to countries in Europe comes from geothermal sources [Wiprut and Zoback, 2000; Buijze et al., 2020; Huang et al., 2020]. Currently geothermal exploration is very expensive [DiPippo, 2012] due to a data intensive process for accurate results.

An obstacle that is often faced during the initial phases of geothermal exploration is the lack of access to accurate subsurface data. Acquiring these datasets is costly and often limited in most areas. This thesis project will focus specifically on fracture data for fracture network modelling. Fractures are commonly found in most reservoirs and there has always been a keen interest on fracture modelling [Lei et al., 2017; Xu et al., 2021; Welsch et al., 2020; Bruna et al., 2019a; Rountree et al., 2012]. There are many different types of fracture modelling, from stochastic to discrete. These types of fracture modelling have high margins of error as the data is insufficient to set reliable input parameters. This study will focus on a geomechanical fracture growth approach that uses insitu stress regime data - which is often already known - to populate a discrete fracture network (DFN). Details into the geomechanical method will be further explained in chapter 4.

A fracture network holds a very important role in determining fluid flow pathways and permeability within the reservoir rock [Shackleton et al., 2005; Rountree et al., 2012; Welch et al., 2022]. Decreasing the unknowns by using reliable geomechanical data and populating a fracture growth model could help decrease the margin of error in fracture network models. This knowledge can contribute to the analysis of fluid flow pathways (permeability) and analyse the effects fractures have on the rigidity of the rock mass. The intended outcome of this work is to provide a three dimensional subsurface fracture model. Authors such as Alhamad [2020], Lo [2019] and Koumrouyan [2019] have done similar investigations. The point of this research is to build on these findings contributing to a stronger understanding of the subsurface.

1.1 GEOTHERMAL PRODUCTION IN SWITZERLAND

The popular use of geothermal energy use in Switzerland started with balneological applications and heat production in the 1980's. From the 1983 to 1998, there were 14 projects drilled to a depth deeper than 400m, ranging between temperatures from 22 to 88 °C [Vuataz and Fehr, 2000]. During the early 2000's there was a shift in focus towards shallow borehole heat exchangers which would be able to provide the heating demand for households in Switzerland. Deep geothermal projects also surged in Geneva, St. Gallen, Brig Zurich and Basel among others. These projects have a rough borehole temperature between 80 and 150 °C [Wyss and Rybach, 2010].

These aforementioned projects were mainly financed and supported by local energy suppliers, this means that the locations of these projects did not follow a

systematic Geothermal Project plan. The location of the geothermal energy projects were largely based on the interests of each party [Wyss and Rybach, 2010]. In order to support and encourage more geothermal energy projects, the government offers a 50% reimbursement of drilling costs in case of failure. 150 million CHF are also reserved in the case of any associated risk of deep geothermal projects [Wyss and Rybach, 2010]. These incentives make it attractive for individual companies to invest in projects to support renewable energy goals. More recently, 27.5 million CHF was budgeted by the government to finance drilling operations in Switzerland [Richter, 2020].

The Swiss Molasse basin covers a large part of the areas with a high population density in Switzerland. It is usually the location for geothermal energy production with gradients of 25-40 °C/km and an average of 60 mW/m^2. Most geothermal energy projects in the region target the Molasse basin [Walch et al., 2021]. Geothermal energy composes roughly 15% of the total energy for heating systems in homes and offices through the use of heat pumps, the goal of the Swiss government is to significantly increase this number by 2050 [Richter, 2020].

1.2 OBJECTIVE OF INVESTIGATION

The aim of this thesis is to use a geomechanical fracture growth modelling approach to assess the fracture network in the carbonate reservoir of the Geneva basin. The thesis project will assess the available data that was provided by the University of Geneva on the GEO-01 well and its surroundings to populate a fracture model. The data that was provided includes optical borehole imaging which will play an integral role in determining the input for the geomechanical discrete fracture network model.

Due to limited seismic data, the orientation of the faults are uncertain. The faults play a major role in geothermal site design and are critical to understanding the mechanisms of the fluid flow pathways. The investigation will assess the fault data and compare it to the analysed fracture data. Through this analysis, there will be a better understanding of the origin of the fractures, which will help populate the fracture network model.

Using an approach that is less reliant on expensive data could help decrease the CAPEX costs of geothermal projects and increase reliability of discrete fracture network models. This investigation will critically look into the benefits and pitfalls of using such methodologies to contribute to the literature on geomechanical fracture growth models.

1.3 CONTEXT OF THE STUDY

The Geneva basin is located in a low relief area between two large mountain chains. The area is targeted for low enthalpy geothermal exploration because it is close to the city of Geneva and can potentially contribute to the city's goal of decreasing their reliance on fossil fuels [Moscariello et al., 2020b; Do Couto et al., 2021]. This is a mechanically active zone with active faults near by, which makes it an interesting case study to assess. Mechanically active zones go through a lot of changes in the subsurface, with varying mechanical properties and insitu stresses. These varying properties are drivers for fracture generation, which makes modelling fractures in this area a complex work.

2 GEOLOGICAL SETTING

2.1 CASE STUDY: THE GENEVA BASIN, SWITZERLAND

The Geneva basin is located in the south western part of the Molasse basin, a low area of relief to the south of the Geneva Lake with the Saleve mountains to the southeast and the folded Jura mountain chain to the northwest (Figure 2.1). The present day landscape of the Geneva basin is composed of three main elements as described by Moscariello [2021]; (i) northwest compression by alpine tectonics, (ii) erosional and depositional features by glaciers and (iii) establishment of the current hydrographical network.

The northwest compression of the Geneva area was a result of anticlinal folds and thrust planes which created strike-slip faults striking southeast-northwest. This compression comes from the two planes that currently make up the folded Jura mountain chain and the Saleve mountain. During this high tectonic activity, glaciers from the Peistocene, have been thought to have shaped the landscape. Evidence of glacier correlated deposits have been found from the Rhone Glacier, Gunz Glacier, Arve Glacier amongst many others. These glaciers occupied the region on and off for the last million years. These long glacial periods left deep and narrow incisions into the Molasse Formation, and deposited sediments along their path. The Rhone river in the present day is very much shaped by the remnants of the effects of the glaciers, leaving behind crevasses and melting waters that make up today's hydrographical network [Moscariello, 2021; Charollais et al., 2013].

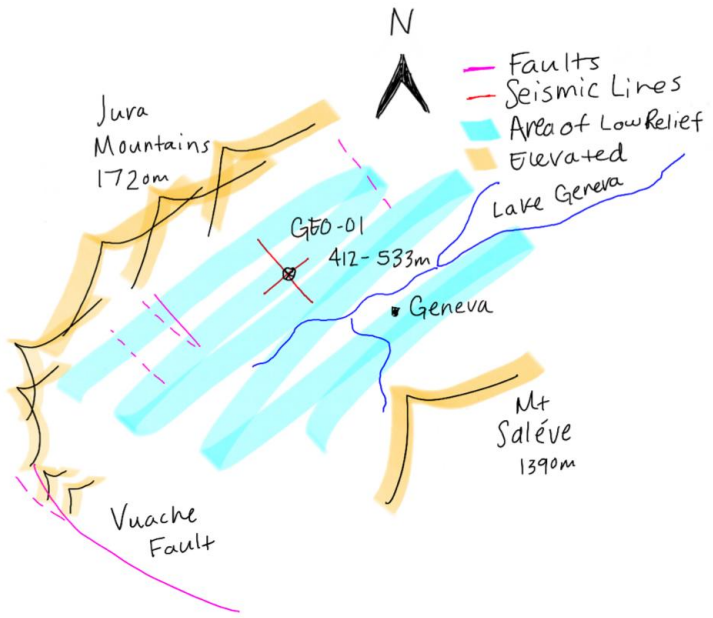

Figure 2.1: Setting the scene for the GEO-01 Well within the Geneva basin

The GEO-01 well is positioned between the Saleve and Jura mountains (refer to figure 2.1) will be used in this study as a point of reference for the area, more

information about the well will come in the section 2.3. In figure 2.2 a cross section is taken from the northwest to the southeast from the Jura mountain chain until the Saleve mountain. In this diagram modified from Moscariello et al. [2020b] there is an interpretation of potential fault locations in the basin and the extent of the geological periods. The basin is relatively close to sea level with elevated mountain chains to the northwest and south east. There is one large fault located towards the southwest of the region called the Vuache fault located near the Vuache mountains in the southwest (refer to figure 2.1). The geological setting shown in figure 5.4 shows that the Molasse Formation in the Oligocene onlaps the Jura and the Saleve mountains, this, according to Moscariello [2021] indicates that morphological highs were already present at the time of deposition. Once this Formation was deposited, it continued to evolve into present day structures [Moscariello, 2021].

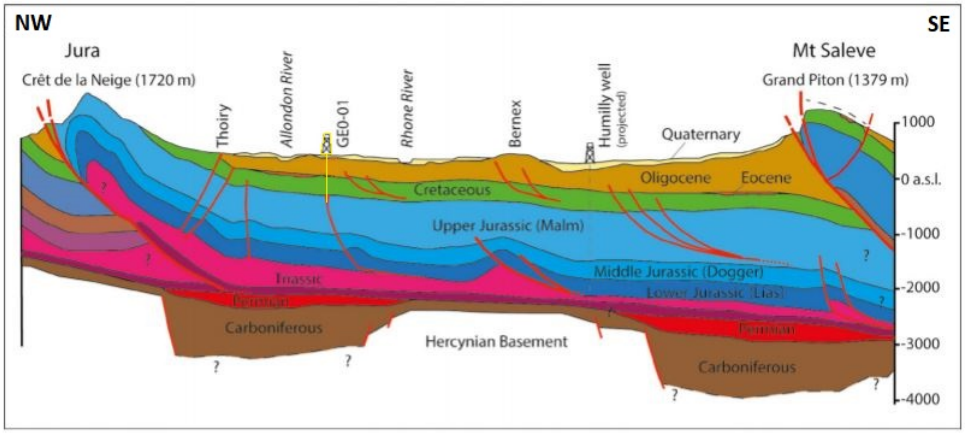

Figure 2.2: Cross section of the Geneva basin showing the location of the GEO-01 well, modified from Moscariello et al. [2020b]

Just within the recent years, there has been a drastic evolution in the understanding of the geomechanical properties of the area (as shown in figure 2.3). Less than 10 years ago it was believed that there were significant fault corridors that crossed through the basin from the NW to the SE. Less than 5 years later, this hypothesis was thrown out and seismic studies gave a clearer understanding of the placement and orientation of large faults. Large and smaller faults were thought to not only be oriented NW-SE, but also NE-SW. By 2019, more smaller faults in the orientation NE-SW were added to the picture creating a different hypothesis for fluid flow. The aquifer recharge is thought to come from the SW according to Moscariello et al. [2020b].

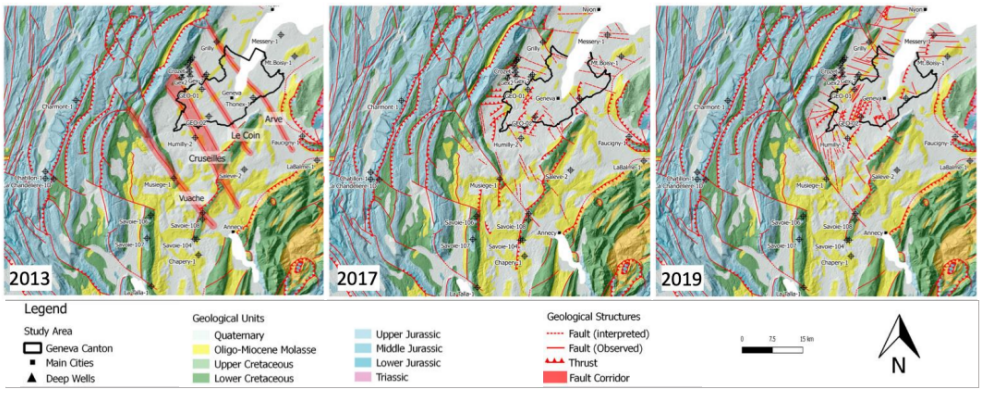

Figure 2.3: The evolution of the understanding of the geomechanical analysis of the subsurface in the Geneva basin (Moscariello et al. [2020a])

2.2 SEDIMENTALOGICAL SETTING

The basin is characterised by the Variscan orogeny resulting from the creation of the continent of Pangea from the collision between Laurussia and Gondwana which makes up the crystalline basement of the Geneva basin [Sommaruga et al., 2006]. The basement is slightly dipping towards the south-southeast and after the collapse of the Variscan belt, Permo-Carboniferous sediments ranging between 3000 - 5000m in thickness [Do Couto et al., 2021; Moscariello et al., 2020b] populated the basin in a series of northeast to southwest oriented grabens. The basin continues with southwest-northeast oriented grabens from the Late Carboniferous marked by clastic sediment deposition, coal beds and dark shales. Shallow marine sediments are later deposited in a period of high sea levels, which are followed by sandstone deposits overlain by carbonates and dolomites from the Muschelkalk and thick evaporites from the Keuper (Lower and Middle Triassic) [Do Couto et al., 2021; Charollais et al., 2013]. Following a marine transgression in the Lower Jurassic marls and shales were deposited preserving organic material. The Dogger and Malm formation follow with shales and limestones from shallow marine environments in the Middle and Upper Jurassic [Do Couto et al., 2021]. The Malm is followed by the Lower Cretaceous which will be the area of focus for this study (as shown in figure2.4).

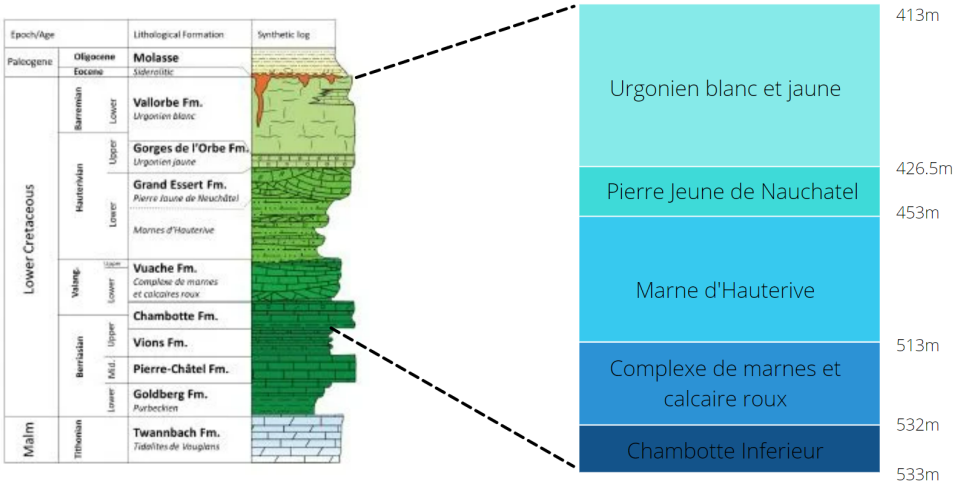

Figure 2.4: Stratigraphic column modified from Charollais et al. [2013]

The Lower Cretaceous is characterised by bioclastic limestones with marly intervals deposited by shallow marine environments through periods of sea level fluctuations. Pelagic chalk and limestone sediments deposited during marine transgression were deposited and later eroded away by the emersion of the Geneva basin leading to karstification of the Urgonien limestones [Moscariello et al., 2020a; Moscariello, 2019]. These bioclastic limestone packages are what characterise the reservoir lithological sequence (refer to figure 2.5). Carbonate platform deposits and bioclastic limestone packages mark the Lower Cretaceous but are absent in the Upper Cretaceous which were eroded in an event that is attributed to the Late Eocene [Do Couto et al., 2021]. The Molasse basin sediments sit on top from the Oligocene made up of mixed fluvial and lacustrine deposits. This Formation onlaps against the Jura and Vuache in the northwest and to the Saleve mountain in the southeast [Moscariello, 2019; Charollais et al., 2013; Do Couto et al., 2021].

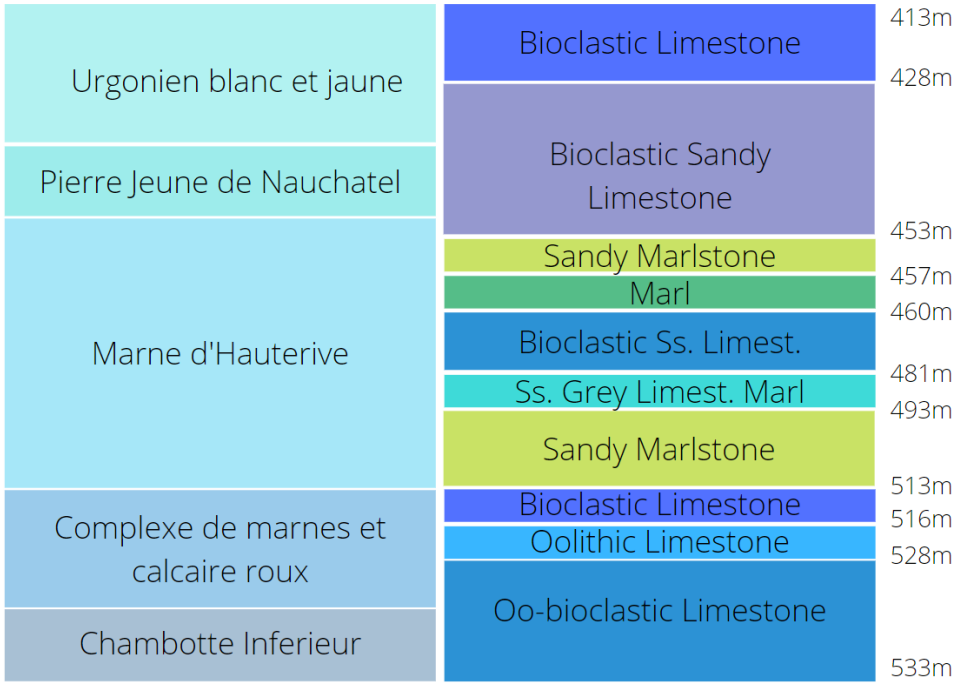

Figure 2.5: Lithological description modified from Chablais and Rusillon [2020]

2.3 GEO-01 WELL

The GEO-01 well was the first well drilled as part of the geothermal initiatives in the Geneva basin, it was drilled as an exploratory well to target the potential reservoir in the upper Jurassic and lower Cretaceous. There has been a lot of work done with the data provided from this exploratory well. The lithological interpretation done by Chablais and Rusillon [2020] will be considered in this study since there is limited access to core data. This lithological description will be built upon using well logging data and other sources [Lo, 2019; Koumrouyan, 2019; Moscariello et al., 2020b; Chablais and Rusillon, 2020; Alhamad, 2020]. A summary of the lithological analysis done for this study can be found in the Appendix A.

It is thought by Moscariello et al. [2020a] that there could be large faults connecting the Permo-Carboniferous rocks to the upper stratigraphic layers. This would be an interesting case for geothermal due to the fact that these fault connections to deeper waters could mean an increase in reservoir temperatures. The GEO-01 well is drilled to a depth of roughly 700m, the interval that will be of interest; is from 413m to 533m TVD. Among the OBI data, there are two interpretation of the fracture data one by Koumrouyan [2019], and another by Lo [2019]. In the interpretation by Lo [2019], there are 469 open fractures and 47 veins, in the interpretation done by Koumrouyan [2019], there are 805 open fractures and 105 veins. These two numbers vary drastically and therefore a new fracture interpretation will be done using the WellCAD [2021] software. This will be further explored in Chapter 5.

The relevance for creating a discrete fracture model for this specific case study is to gain a better understanding of the mechanics and fluid flow pathways of this reservoir. Figure 2.6 shows the hydrological recharge of the subsurface in the Geneva basin, and the potential uses for geothermal. Borehole heat exchangers and heat storage, hydrothermal or enhanced geothermal systems could be incorporated into this system in order to decrease the reliance on individual boilers that use gas, and increase the share of district heating within the city of Geneva [Moscariello et al., 2020b,a]. The forecast for the Canton of Geneva in 2035 is that there is a

higher reliance on waste heat, geothermal and heat pumps (for low temperature geothermal) to feed a growing district heating network. To help realise this future, the ability to recreate the conditions in the subsurface are crucial for optimal performance of the potential geothermal doublet system.

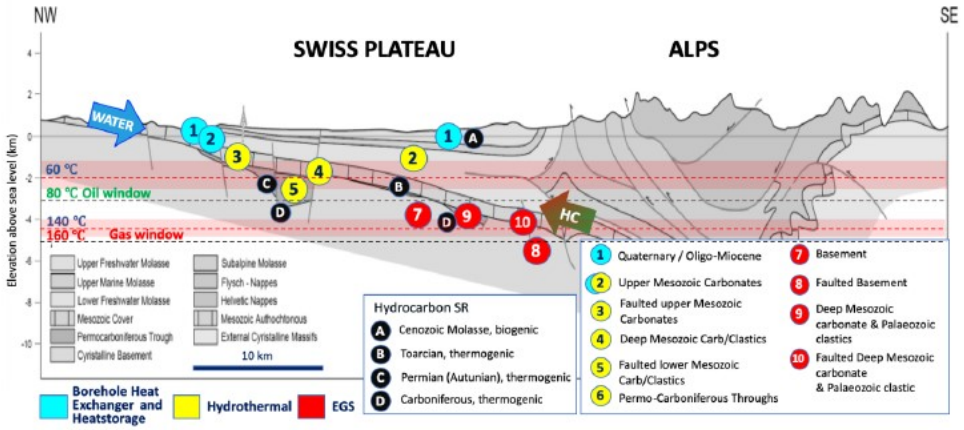

Figure 2.6: Hydrological pathways in the subsurface modified from Moscariello [2019]

3 MECHANICAL FAILURE

To be able to identify and predict fracture patterns in the subsurface, the mechanisms behind fracture formation need to be identified. This chapter outlines the basics of mechanical rock failure and fracture formation. This section will cover the basics behind rock mechanics, stress and strain relationships, and deformation. The types of fractures and stress regimes that could create different types of fractures will also be briefly explained.

3.1 ROCK MECHANICS

The mechanical properties of the rock depends on the amount and type of fluid as well as the amount of void space available in the rock matrix. The permeability is controlled by the size and connectivity of the void, viscosity of the fluid, density and temperature [Notre Dame, 2020]. Pressure is defined as the force applied by a load per unit area, while stress is the pressure that is being transmitted from the outside of the load to the inside (also as force per area). To measure the stress on any load, the stresses can be divided into three principle stresses; σ_1, σ_2, and σ_3. The amount of stress that a rock can take before it breaks is influenced by the mechanical properties of the rock. Fractures and faults in the rock represent points in which the stress has caused the rock matrix to break, reaching its point of inflection.

When stress is applied to a rock formation, the formation begins to deform and yield. Strain is defined as the change in length divided by the original length of the formation. The relationship between stress and strain is known as the modulus of elasticity ($E = \frac{stress}{strain}$). In rocks the formations begin to deform as the stress and strain increase. There is a point where the point of failure where the rock formation breaks (point of failure). The breaking of a rock could result in either small fractures or one large fault depending on the scale of the pressures and the combination of directional stress applied to the rock mass. The type of fracture that is formed depends on the stress regime applied on the rock face, this can be seen in figure 3.1.

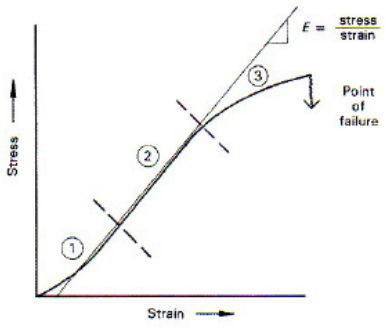

Figure 3.1: Stress and Strain relationship and regions of deformation from Notre Dame [2020]

When stress is applied, the rock begins to deform and depending on the pressure applied, the rock behaves in various ways. Referring to figure 3.1, the first

region on the graph - where stress and strain is low - is where the void spaces in the rock begin to close, the second region is approximately where most elastic behaviour is observed, region 3 is where plastic behaviour may be observed, and finally the point of failure, where the rock loses all its shear strength.

Referring to figure 3.2, the diagram shows the affects of temperature and pressure on the ductility and brittleness of the rock formation. This shows that ductility increases with confining pressure and temperature and how initial elastic behaviour is seen in all cases. The diagram also shows that there brittle deformation happens in the form of fractures in the rock, while during ductile deformation plastic behaviour is observed. With increasing temperature and pressure the rock shows a more plastic behaviour where the matrix will morph instead of rupture. The rock usually follows elastic behaviour until the point of inflection when a failure in the rock causes a fracture or a fault. There can be multiple potential fracture points along the grains of a rock matrix, these grains are randomly oriented and fracture when there is high tensile stress at the grain boundary. This can be later applied by using the presence of fractures as an indicator of the presence or absence of plastic ductile behaviour [Lonergan et al., 2007; Rountree et al., 2002]. This helps to indicate the paleo stresses that were active on the rock formation over the years. This can be useful in indicating the possible fluid flow pathways that could remain active for geothermal production.

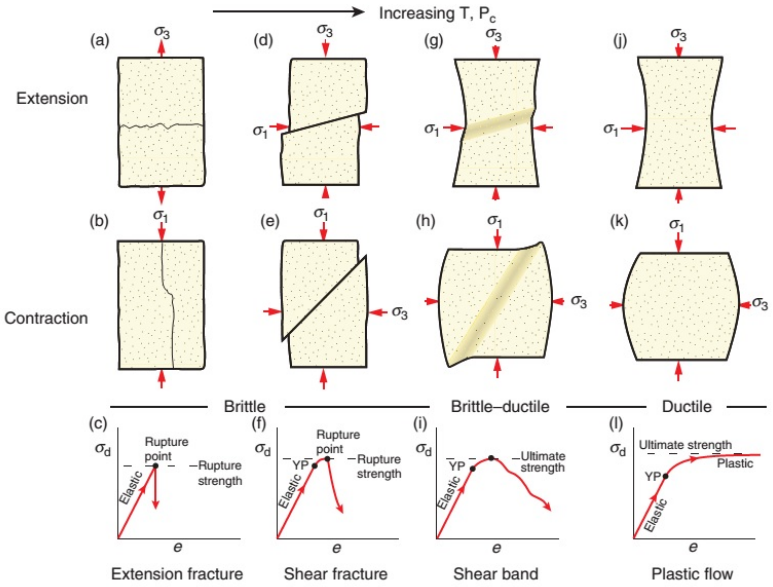

Figure 3.2: Experimental deformation structures that develop under extension and contraction adapted from [LearningGeology, 2015]

3.2 FRACTURE TYPES AND STRESS REGIMES

When referring to fractures in the field, there is some debate as to how to classify them. There is a consensus that there are two main types of fractures; mode I- opening (extension, also known as joints) and mode II- (sliding) shear perpendicular to the edge. However, in some literature, there is a mode III- (tearing, also known to be stylolite compaction bands) slip parallel to the edge [O'Brien and Hodgins, 1999; Xueliang et al., 2018] which to some authors is considered as a separate mode while other others such as Floros et al. [2015] and Shlyannikov et al. [2021] consider the third mode to be a mix between mode I and mode II. There is also a mode IV fracture- (closing) contractional fractures such as stylolites that is being classified as

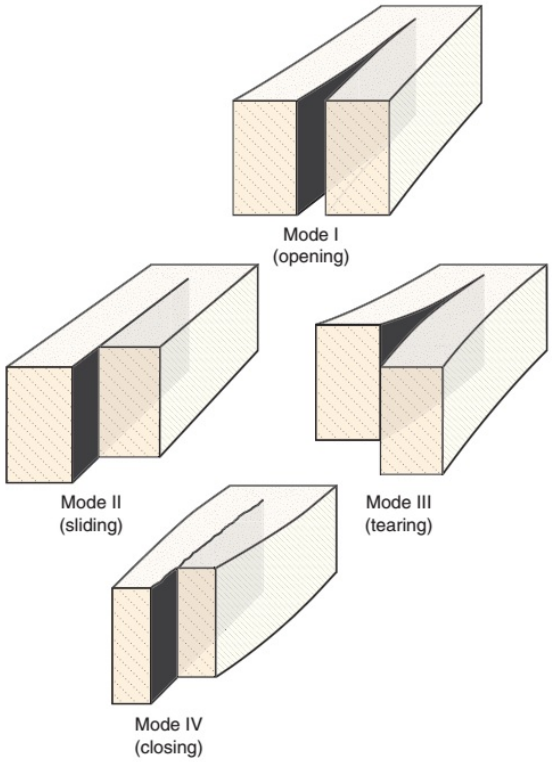

Figure 3.3: Fracture modes; Mode I (Joint), Mode II (sliding) and Mode III (tearing) and Mode IV (Stylolites) [LearningGeology, 2015]

a closing fracture [LearningGeology, 2015]. The extensional fractures develop under low confining pressure and perpendicular to σ_3. Shear fractures develop roughly 30 degrees from the σ_1 commonly develop in conjugate pairs.

Fractures represent the concentration of void space in rocks which means that they change the permeability (connectedness) of the pore space. The size, orientation and dip of the fractures control the fluid flow of the reservoir. The geometry of the void is controlled by the precipitation of minerals, geological origin of the fracture, and changes in regional stress [Long et al., 1996]. The voids the fracture creates make up a network of interconnected pathways. In low permeability reservoirs, the permeability can be changed through fracturing, where fluid flow pathways can be increased in some directions.

The presence of a fracture network within a rock mass has an effect on the over all strength of a rock and the density of the fracture network can have an impact on the point of failure of a certain rock mass in hydrothermally altered rock [Wyering et al., 2017; Hoek et al., 1995]. Having a discrete fracture model that can closely predict the conditions in the subsurface can help in assessing how much pressure a rock mass can take. This becomes very relevant when drilling, injecting and producing from fractured rock as unknowns can cause rock breakage [Voigt, 1966; Zoback and Kohil, 2019; Hoek et al., 1995; Stead et al., 2015].

Figure 3.4 shows the possible combination of mechanical fracture types and stress regimes, and how different magnitudes cause different fracture shape and angle. The three main scenarios for the propagation of extensional fractures in tension, shear fractures and extensional fractures in confining pressure [Maerten et al., 2016]. What this image does not show is the variations in fracture roughness which affect the properties of the void spaces [Brown and Scholtz, 1985]. The roughness of the fractures will have an effect on the analysis of the voids spaces created by fractures. This analysis can be used to calculate the aperture using relationships established

by Barton et al. [1985]. From the calculation of the aperture, the permeability can be calculated using a modification on the classic Karman-Cozeny expression. This will be further expanded upon in Chapter 4.

When using fractures to beck calculate the stress regimes, figure 3.4 can be used to deduce the stress regime active at the time. This would be useful to calculate the paleo-teconic stresses required during geomechanical analysis of the subsurface and will be used to populate a geomechanica DFN in chapter 6.

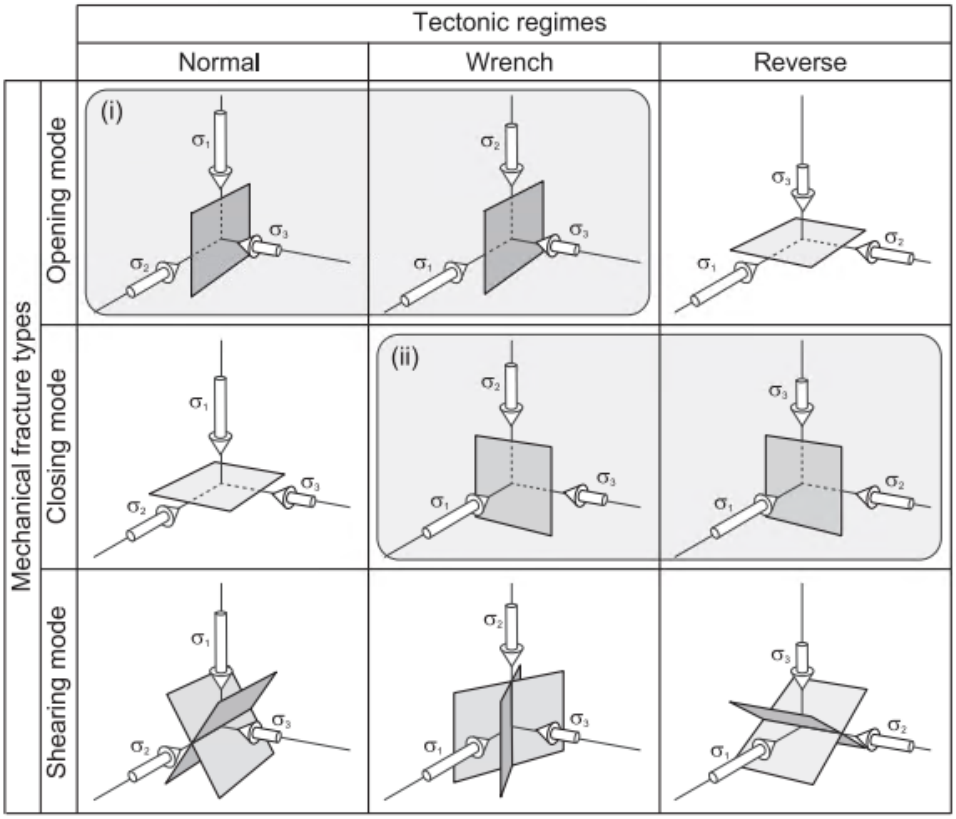

Figure 3.4: Fracture modes; Fracture responses to tectonic regimes for three mechanical fracture types (shearing, closing and opening modes) (i) and (ii) represent the two stress ratios that could be confused under Andersonian regimes [Maerten et al., 2016]

3.3 STRESS DEVELOPMENT IN GEOTHERMAL RESERVOIRS

In-situ stress is a set of far-field mechanical forces impacting underground structures. There are four types of in-situ stresses: gravitational, tectonic, residual, and terrestrial stresses. The gravitational and tectonic forces produced by the motion of crustal plates are the main sources of in-situ stresses [DiPippo, 2012; Min and Kim, 2012; Radwan and Sen, 2021]. In-situ stresses within the earth's crust are typically defined in terms of principal stresses and their orientations. The in-situ stresses are classified as normal fault (NF), strike-slip (SS) and thrust fault (TF) stress regimes depending on whether the magnitude of the vertical stress is the largest, intermediate or the least [Min and Kim, 2012]. These are the basic theories behind the Andersonian Model. Knowing the principle stresses, can help determine which of these three scenarios are most likely to have occurred. This can give insights to the direction and orientation of the faults which could also help with well placement in a reservoir.

4 FRACTURE MODELLING TECHNIQUES

4.1 METHODS FOR MODELLING FRACTURES IN THE SUB-SURFACE

In the early days of fracture modelling there were limited variables to tweak. A house of cards approach (continuum methods; equivalent porous media, stochastic continuum) which make up a uniform grid block of a square three(or two)-dimensional matrix is a simplified version of modelling fractures [Karimi-Fard et al., 2004; Liu et al., 2008]. This created the first interactions between matrix to fracture and fracture to fracture flow in terms of meshed elements. In these models, the density and the direction were controlled but there was little variation between individual fractures. The limitation to these methodologies is that the fractures were too streamlined. In a model to represent fracture flow, the travel time of the fluid at any point on a single axis would be equal. When in reality the rock mass is heterogeneous, with changing fluid flow pathways along the column [Rountree et al., 2012].

An approach focused more on the modelling of the individual fracture are the discontinuum methods which include infinite fracture models (box of confetti), channel network modelling and discrete fracture network modelling. Xu et al. [2021] have outlined visually the difference between different approaches to fracture modelling. Categories include spatial subdivision, DFNs, geostatistical approaches [Zhang et al., 2019], multi-point statistical approaches [Bruna et al., 2019a,b], iterations of fractal characteristics and seismic event point cloud.

The spatial subdivision and the geostatistical approach are implicit stochastic models with limited data to populate the fractures. The data is also heavily deterministic using the Terzaghi method to approximate spatial unknowns, this increases the uncertainty of the populated fracture model [Welsch et al., 2020]. The Fracman modelling approach is a discrete fracture network for modelling geometrical characteristics and populates the fracture network using geometrical representations of the individual fracture [Lei et al., 2017]. A draw back to this approach is that the features do not represent the fractures, but aim to represent the statistical variation of the fracture network which could cause discrepancies in predicting fluid flow and low scale permeability.

A relatively new method for populated DFNs is to model the fracture growth over time using geomechanical properties. The benefit of this method is that the geomechanical properties of a rock mass are often known, and can be used along with static properties of the rock to predict the type and amount of fracture growth in a certain area [Welch et al., 2022; Welsch et al., 2020]. This approach differs from the stochastic DFNs by generating statistical fracture data through the simulation instead of being predetermined. The geomechanical fracture growth approach to fracture modelling is the fracture growth approach that will be used for the purposes of this study.

This discrete fracture network model using geomechanical properties does not need extensive and expensive data from coring, but can use existing mechanical data to create insitu stress conditions to simulate the fracture propagation. A lim-

itation to this method is the ability to handle only a single stress event; to the modelling of fractures in the rock mass attributed to a constant strain and stress magnitude. If the stress magnitude and direction would change creating new fractures in the rock mass, two separate DFN models would need to be run. This will be further investigated in chapter 7.

4.2 VARIABLES IN DISCRETE FRACTURE MODELS

Fracture modelling is complex, with a lot of variable geometrical properties [Rountree et al., 2012];

- Orientation (dip and dip direction)
- Shape
- Density (actual P20 and apparent P30)
- Spacing or frequency (P16)
- Intensity (actual P21 and apparent P32)
- Diameter (aperture)
- Location
- Length

Some of these variables can be estimated using the data available, but others are a modelling choice, and will have an effect on the output of the discrete fracture network. Orientation and dip are two variables of high importance when looking at determining fluid flow pathways and therefore can propagate high margins of error in the output model. Shape is a choice that is often model specific each modelling approach takes a fracture and models it as a circle, triangle, rectangle or polygon.

Density (m^2), spacing and intensity (m^3) are often controlled using outcrop data, or well data by counting fractures within an area or length [Niven and Deutsch, 2010]. Density in the case of the geomechanical fracture growth approach is considered to be a factor of the stress/strain relationship, as well as the stress shadow (this will be further explained in section 4.3).

Aperture of a fracture in stochastic models is often a statistical value with some boundary conditions, the geomechanical modelling approach uses the orientation of the fracture to predict the aperture together with the orientation of the principle stresses [Welsch et al., 2020]. Location and length of the fracture propagation in the network is determined by the method of modelling, depending on whether the model is stochastic or deterministic. Within the context of the geomechanical model, the new fractures are placed randomly around the grid, and are grown over time using layer confinement and tress shadowing as boundary constraints. This will be explained in further detail in the following section.

4.3 GEOMECHANICAL FRACTURE GROWTH MODELLING APPROACH

The geomechanical fracture growth approach used in this study is that described by Welsch et al. [2020] and will henceforth be referred to as the geomechanical fracture growth DFN (G-DFN). This is a plug in that can be used in combination with Petrel to model fractures within a predetermined grid block. The G-DFN works in k-layers which divide up the grid block vertically. These k-layers are predetermined through

an analysis of the mechanical properties of a reservoir, making the differentiation between soft and stiff layers. In figure 4.1a the G-DFN is shown populating a brittle layer with fractures with controlled insitu stress parameters. These fractures are confined to that brittle layer allowing for a variation in fracture properties in other mechanically varying reservoir packages.

This modelling method uses a mesh and node system with constraints and parameters in order to create a fracture network that develops and grows over time. The idea behind this fracture generating method is to use a node within a mesh to generate one fracture at a time at locations determined by a random number generator. Newer fractures will then develop over time with respect to the older fractures present in the model (refer to figure 4.1b).

Referring to figure 4.1b, this image describes the time sensitive fracture propagation of populated fractures in the model. The orange circles represent microfractures which remain circular until they have expanded to the full confines of the layer. The propagation rates of these microfractures are determined using the subcritical fracture propagation theory. When the microfractures reach the limits of the layer, they become macrofractures [Welsch et al., 2020]. The purple rectangles represent the macrofractures and have a constant height propagating only laterally. The G-DFN propagates fractures through time from both lateral tips as shown by the markings "LT" in figure 4.1b. The propagation will stop if the growing fracture reaches the stress shadow zone of another fracture shown by the markings "A" and "B" in the figure. The model runs for a set length in time and outputs a single layer of a "naturally" distributed fracture network.

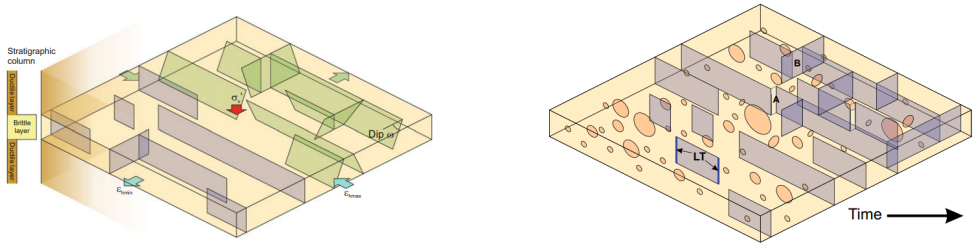

a b

Figure 4.1: (a) Fractures generated by the G-DFN constrained by mechanical properties of the rock and controlled by insitu stress regimes (a) G-DFN model of individual fracture growth over time adapted from Welsch et al. [2020]

The G-DFN has the ability to integrate the deformation by time-dependent inelastic processes, in a viscoelastic model, horizontal strain remains constant. As the model runs, the strain accommodated on the fractures will increase [Welsch et al., 2020]. The G-DFN will then recalculate the insitu stresses at the beginning of each timestep iterating any time related stress changes. In the event of temporally varying mechanical properties in the rock mass, the model has a limitation as mechanical properties of each layer remain constant throughout the run time of the propagation event.

The rigidity contrasts of individual rock layers in a package control the confinement of fracture networks [Shackleton et al., 2005; Underwood et al., 2003; Helgeson and Aydin, 1991]. Figure 4.2 shows four different scenarios of fracture confinement between beds. Scenario A has a high rigidity contrast between beds, with fractures confined only stiff rock layers. Scenario B has low contrast rigidity where the fractures are not confined to the beds. Scenario C and D show cases where the mechanical properties (rigidity) of the rock have evolved over time showing the presence of both confined and unconfined fractures. This suggests that the rigidity ratios between beds are temporally varying.

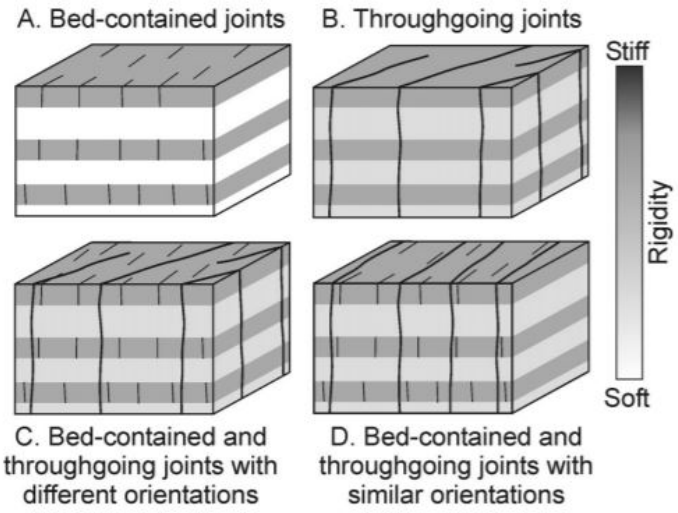

Figure 4.2: Fracture stratigraphy vs. mechanical stratigraphy; how some fractures can be cross bedding while others are confined, an interesting concept to be applied to the Geneva basin case study adapted from Shackleton et al. [2005]

Using the G-DFN to model these would require the superposition of two separate model runs, one with a scenario where fractures are not confined by beds, and the other with high rigidity ratios where fractures are bed confined. The changes in mechanical properties could also mean changes in stress magnitude, which could result in fractures being formed under varying conditions. This aspect will be further investigated in chapter 7.

4.4 UPSCALING

One of the major uses for modelled fracture networks is to upscale the fracture properties to be used in fluid flow simulation modelling. This is especially useful in tight rock reservoirs where the matrix permeability is low, and the fracture network will effect the connectedness of the reservoir. The presence of a fracture network can increase the permeability in reservoirs allowing for high flow rates of brine to the subsurface. This is relevant for low enthalpy geothermal when higher flow rates can distribute more heat power. Fracture permeability is not the only advantage to upscaling fracture networks, but the understanding of the matrix of the network can help to predict the rigidity and strength of a rock, this can have implications on pore pressure and help to lay constraints on reservoir management.

Fracture modelling can help in indicating areas which are more sensitive to drastic pressure changes and therefore at risk of reactivation. A high risk of seismicity comes with subsurface projects that are close to large faults that may be reactivated when pressures reach certain thresholds [Gupta and Chadha, 1995; Chandrasekaram and Bundschuh, 2008; Moeck et al., 2009]. This falls especially into the high risk category when geothermal projects are producing from fields near populated urban areas. Although in most cases geothermal production has been running for years without any induced seismicity [Shapiro, 2015; Zoback and Kohil, 2019; DiPippo, 2012; W.A. and Pascher, 1996], there have been some cases in which the induced seismicity effects have cause the projects to shut down [Mignan et al., 2015; Haring et al., 2008; Zoback and Kohil, 2019; Trifu, 2002]. The effects of seismicity can occur due to inaccurate geomodelling of stress regimes of the project location which can then create unsafe operating injection and production boundaries [Wiprut and Zoback, 2000].

5 DATA AND MODEL PREPARATIONS

The initial data gathering and validation uses 2D seismic lines, which tell very little about the orientation of the faults. The orientation of these faults is crucial in determining the paleo-tectonic stresses present during formation, which have a direct effect on fracture growth. The orientation plays a key role in determining the stress regime active in the area. Due to the fact that there is little accuracy as to the orientation of the faults, a larger emphasis will be placed on the fracture data when building the fracture model. This will be the main difference between the model proposed by Alhamad [2020] which relies on fault data to calculate the paleo-stress inversion.

The raw data consists of two seismic lines oriented in northwest-southeast and southwest-northeast, and a combination of well logs that include; OBI, gamma ray, resistivity, sonic and neutron porosity. The seismic data will allow for an in depth look at possible horizon depths and geometries, and an idea of possible fault locations regarding the well. A fault analysis identifying the different fault models by Lo [2019] is used as a base to further investigate the seismic in more detail and identify prevailing faults. For simplicity please refer to the flow chart in figure 5.1 for an overview of the choices that were made in this thesis.

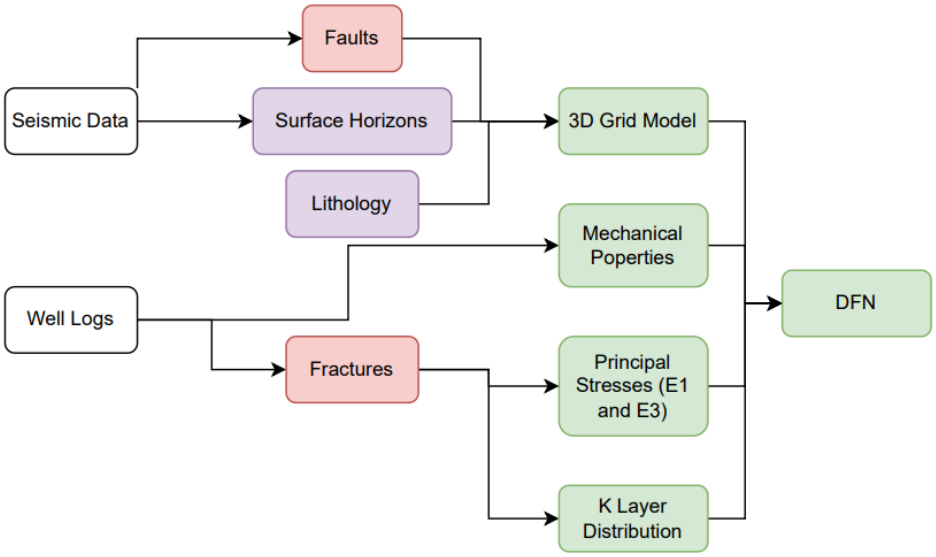

Figure 5.1: Flow chart of all the data that was used, analysed and calculated in this work; All white boxes are raw data taken in, purple boxes are analysed data that was taken as a given from other sources, red boxes are data that were reanalysed and used, and green boxes are data that were calculated

Using the combination of the raw seismic data along with the horizon interpretation, fault interpretation, a structural (3D grid) model will be created and used as input for the the fracture growth model. The interpreted data is made up of the lithological description by Chablais and Rusillon [2020] which comprises of a very detailed centimeter scale description of the reservoir interval refer to Appendix A for a summary of the lithological description.

5.1 SEISMIC DATA

The seismic horizon interpretation was already provided by the work of Clerc et al. [2016], Lo [2019] and Moscariello et al. [2020b], here they identified the five different Formations that will be used in this investigation outlined in the table 5.1 below. The currently available seismic data for the Geneva basin study area are two 2D seismic lines oriented in the NE-SW direction and NW-SE direction. The interpretation done by Clerc et al. [2016] defines the upper and lower limits of the Urgonien blanc et jaune, Pierre Jaune de Neuchatel, Marne d'hauterive, Complexe de marnes et Calcaires Roux, and Chambotte inferieur. The depths of these surfaces along the GEO-01 well log are inline with the interpretation done by Chablais and Rusillon [2020]. The geometries of the horizons also follow a logical trace along the seismic. This was verified using two different types of seismic attributes; (i) root mean square amplitude and (ii) the relative acoustic impedance.

Horizon Top	**Depth at GEO-01**
Urgonien blanc et jaune	413m
Pierre Jeune de Nauchatel	426.5m
Marnes d'Hauterive	453
Complexe de marnes et calcaire roux	513m
Chambotte Inferieur	532m

Table 5.1: Outlining the 5 horizons used in the seismic data to build the static model [Lo, 2019; Clerc et al., 2016; Moscariello et al., 2020b]

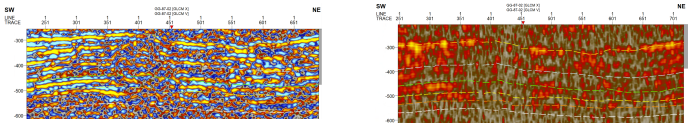

(a) (b)

Figure 5.2: Horizon interpretations by Clerc et al. [2016] for reservoir interval (a) Relative Acoustic Impedance (b) RMS Amplitude

5.2 FAULT ANALYSIS

The faults are only visible on the seismic line oriented in the NW-SE direction. The interpretation by Lo [2019] (shown in figure 5.3a). Using seismic attributes such as dip illumination, edge evidence and first derivative, a new fault interpretation was done (shown in figure 5.3b). After careful examination of the data using different seismic attributes, zones of displacement shown in the seismic had a higher correlation to faults in figure 5.3b. This interpretation also corresponds to the findings in the paper published by Perozzi et al. [2020]. Using the new fault interpretation, along with the existing seismic horizons, a structural grid can be created. This structural grid will be the base of the fracture network modelling described in chapter 6, providing a differentiation between formations and locations of possible faults.

A conceptual scheme of the GEO-01 well from Koumrouyan [2019] shown in figure 5.5 suggests that there is a fault that crosses the well. Similar conceptual diagrams are seen in Moscariello [2021]; Moscariello et al. [2020b]. This aligns with the fault model shown in figure 5.3a. However at this point, this investigation has found no data which corresponds with the assumptions made in this conceptual model, and therefore will chose to omit the faults that cross the well and validate this choice using OBI data which will be further discussed in section 5.3.

The modelling of large faults in the Geneva basin is a relatively open ended as shown in the figure 5.4. The figure shows different techniques such as machine learning to identify fault zones within the reservoir interval. This differentiation between this image and the figure 2.3 in chapter 2 shows that there are some discrepancies in fault modelling in the Geneva basin. There are multiple interpretations and views as to what the orientation and placement of these faults are.

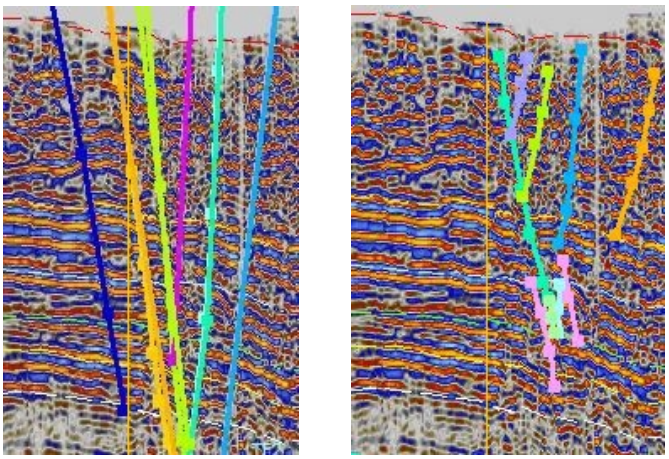

(a) (b)

Figure 5.3: Fault interpretations for varying fault models along the NW-SE dipping seismic line (a) Fault interpretations by Lo [2019] (b) Fault interpretations of this study

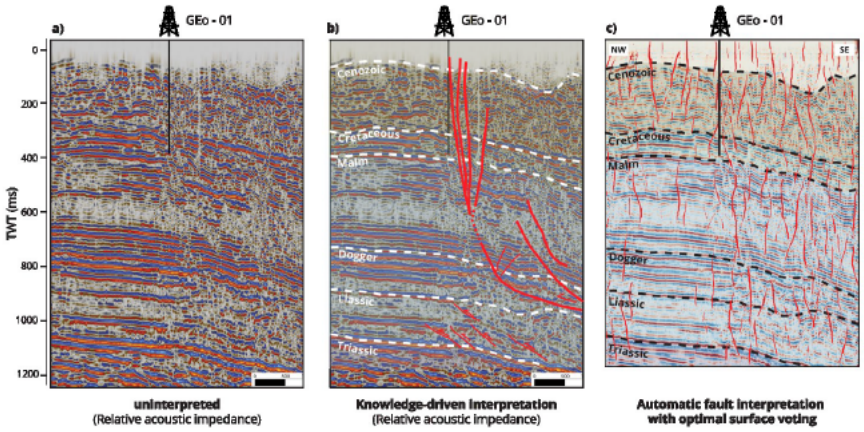

Figure 5.4: Interpretation of faults around the GEO-01 well by Perozzi et al. [2020] showing the different seismic imaging tools used to identify faults, where the interpretations do not show any faults crossing the GEO-01 well

In order to use these faults in the model, they will need to be converted into fault surfaces. There are only two 2D seismic lines available to model the fault surface interpretation, therefore it will be difficult to assess their orientation. The lateral direction can be predicted via seismic, but the extent of the faults perpendicular to what is shown on the seismic it still unknown. As mentioned before, because there is a high uncertainty on the orientation of the faults the fracture growth model will rely more on the fracture data from the OBI to populate the model.

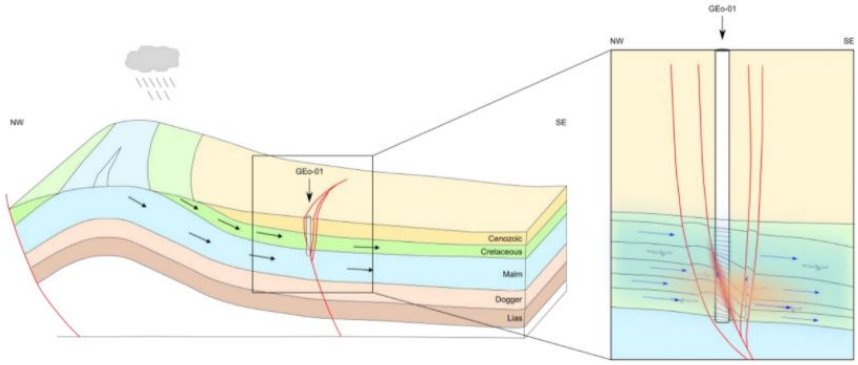

Figure 5.5: Interpretation of cross section of GEO-01 well found in Koumrouyan [2019] with similar conceptual models found in Moscariello et al. [2020b]; Moscariello [2021]; Lo [2019]

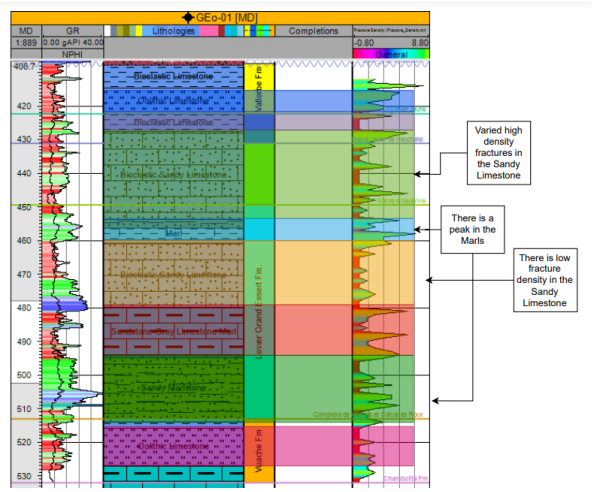

Figure 5.6: Assessing fracture distribution; Lithology is shown in the wide column in the middle, and seems to roughly correspond with the fracture density readings on the right.

5.3 BOREHOLE DATA

This data includes various well logs specifically; density, gamma ray, sonic velocity, caliper and OBI. The gamma ray and density logs will be used to determine the mechanical properties of the subsurface along with the sonic velocity to determine the Young's Modulus and the Poisson's ratio, which together with the fracture density will help to predict the differentiation between stiff and soft layers.

The open borehole imaging raw data has been provided in the data package along side a very detailed analysis done by Koumrouyan [2019]. This very in depth analysis has detected 544 fractures, 261 bedding marks and 159 veins. This was done using WellCAD [2021], the analysed data has also been provided as part of the data package and will be used as a base to re-assess the fracture picks. This number is very different from the number picked by Lo [2019] of 212 fractures using the Technolog software to pick fractures. The difference comes from the focus of Koumrouyan [2019] on very detailed picking fractures. Some of the pickings done in this study could have resulted from bedding that could have been mistaken for a fracture. This large discrepancy has motivated a further look into the OBI data. This is necessary seeing as this OBI characterisation will play a major role in the base for the fracture model.

5.4 ASSESSING FRACTURE DISTRIBUTION

Assessing the distribution of fractures in a reservoir requires a number of assumptions. These assumptions need to be made carefully as choosing to make an assumption will significantly affect the outcome of the model. In this section, the work flow of the assumptions made in this fracture growth model model will be explained and justified using examples from the data.

Looking at the fracture density log interpreted by Koumrouyan [2019], there are some discrepancies between fracture identification and bedding. There are some low angle fractures that could be bedding and not fractures. The fracture veins (closed fractures) are also classified and will also be used in the fracture modelling. The modelling can later be modified to distinguish between closed and open fractures for fluid flow calculations.

This analysis identified three main differences between the analysis of Koumrouyan [2019]; (a) 31 low angle fractures could be mistaken for bedding at 527 to 531m (b) 23 less fractures in the lower part of the marl section between 504 and 515m, (c) 10 bedding marks mistaken for fractures 499 to 503m (d) 27 less fractures in the bioclastic sandy limestone between 470 and 480m (refer to figure 5.7). From this the fracture density patterns per meter can be used in petrel to continue preparing the inputs for the fracture growth model.

The analysis will be done using the same characterisation tool as done by Koumrouyan [2019], the WellCAD software. This software allows for a manual fracture picking and offers the ability to differentiate between veins, bedding and different types of fractures.

The first step in the cleaning of the fracture data was the removal of the low angle fractures. This is due to the fact that low angled fractures have a high likelihood of being mistaken for bedding. Bedding in an FMI could be mistaken from a fracture due to the fact that the FMI is a 360 degree picture of the well. This means that bedding with a slight tilt could be mistaken for a fracture with the same wave like characteristics of a fracture pick. It is very difficult to determine whether or not the pick is a fracture or a bedding, so as shown at the top of the cross section in figure 5.8, the low angled fractures ($<$ 10 degree dip) were removed from the picked data. Veins and fractures were distinguished based on the presence of cement. In fractures where there was a lighter color tracing the fracture, this fracture was considered cemented, and therefor classified as a vein.

5.5 FRACTURE DATA

After a thorough look into the OBI data, there was no clear evidence of displacement within the borehole. This could mean that there are no faults crossing in that area. Other brief observations from the fracture picking data are that the fractures are indicative of a normal faulting stress regime with sub vertical dips and polymodal behaviour. Specifically in the Marne d'Hauterive where there are two poles dipping at 60 degrees. This is a classic normal faulting behaviour. Looking at the other formations, the orientation of the fractures seem to turn clockwise from 0 degrees at Urgonien, 60 degrees at Pierre Jaune de Neuchatel, 120 degrees at Marne d'Hauterive and 180 degrees at Complexe de Marne er Calcair Roux. This is different to the fact that the faults are thought to be strike slip [Moscariello et al., 2020b; Do Couto et al., 2021; Koumrouyan, 2019]. This could indicate that the fractures and the faults were not created by the same event.

Referring back to the figure 3.4 taking into consideration the fracture patterns observed, the shearing mode normal fractures could be applied in this case. The

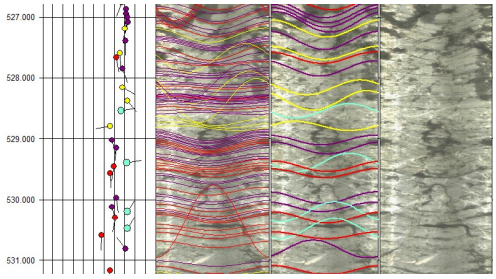

(a) Some fractures could be bedding

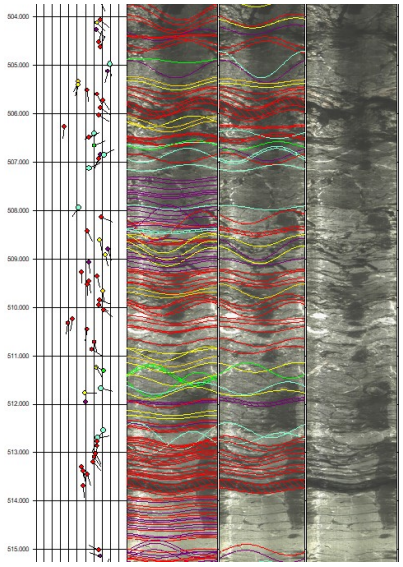

(b) High fracture intensity in Marl

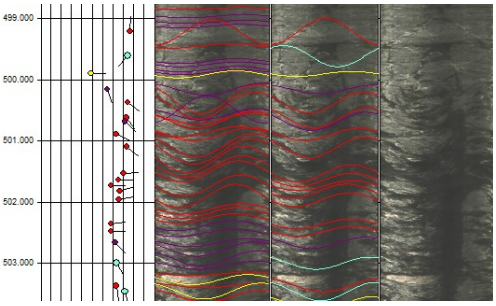

(c) Some fractures could be bedding

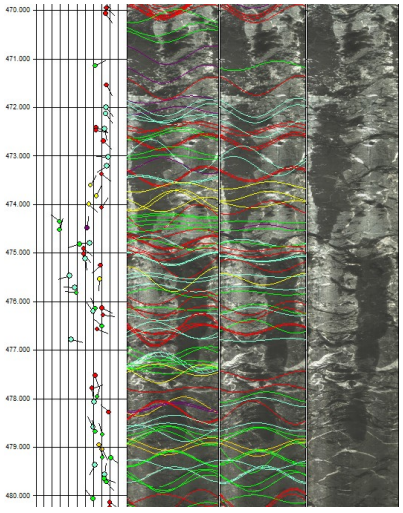

(d) High fracture intensity in bioclastic limestone

Figure 5.7: Differences in fracture picking comparison with Koumrouyan [2019] for more details see Appendix B

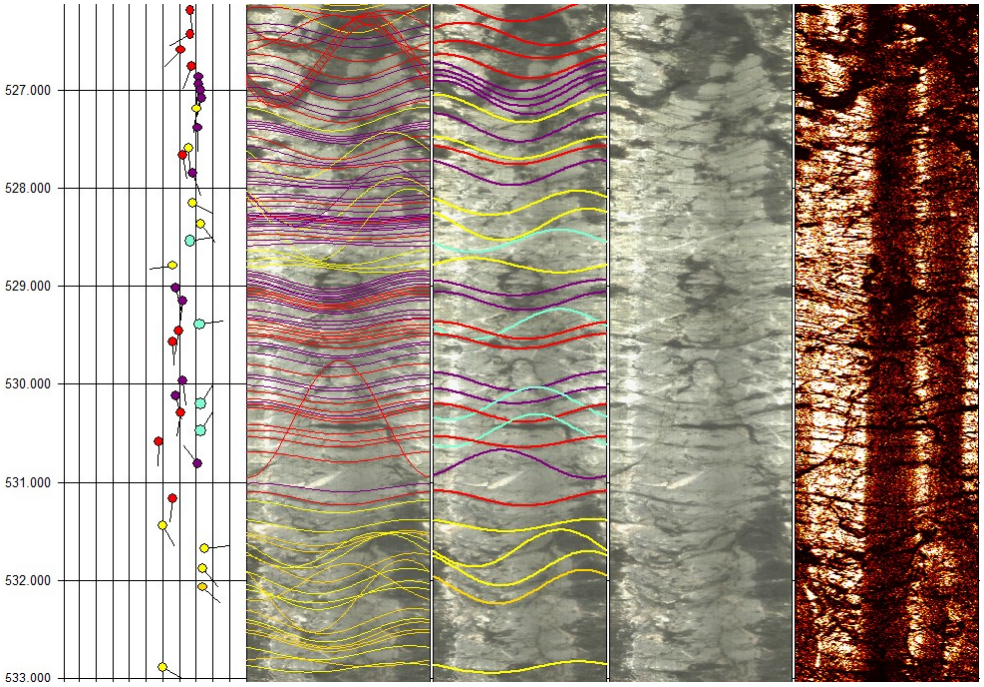

Figure 5.8: Fracture picking comparison between Koumrouyan [2019] on the left and the current interpretation on the left. For more example refer to the Appendix B

rotating orientation could be due to a rotating sigmaH which could control the orientation of the fracture growth. The associations that can be made with the fracture patterns shown in table 5.2 is that most of these fractures were formed under normal stress conditions due to the dip angle being roughly 60 degrees. It can also be seen the orientation of the fractures seems to turn with depth, with the open fractures in the Urgonien blanc et jaune oriented towards the northwest and each formation below adding roughly 30 degrees to the right. This could be due to a shifting max horizontal strain.

The majority of the open fractures seem to accumulate in the center areas of the reservoir with Pierre Jaune de Nauchatel, Marne d'Hauterive and Complexe de marne et Calcaire Roux with the main part of the fractures per meter. Chambotte inferieur has the least amount of fractures per meter, but is also the smallest formation. Urgonien blanc et jaune and Chambotte inferieur also seem to have very similar orientations in the NE-SW directions, as well as Marne d'Hauterive and Complexe de marne et Calcaire Roux.

When looking at the veins or closed fractures, it can be seen that there is difference not only in dip but also in orientation within formations. This could suggest that the veins were formed previous to the formation of the current open fractures and the strain field has since then changed. This can be seen from some cross cutting happening in the OBI data, an example is shown in figure 5.9

Referring to figure 6.1 of all open fractures and figure 5.11 all veins, there is a pattern of polymodal fracturing. Polymodal fracturing is a term that has been used by Healy et al. [2015] for use in classifying fracture orientation patterns. Polymodal fracturing has been validated in labs and in nature that one set of fractures can produce a wide 'butterfly' range of orientations. Strain is being pushed onto the rock face from three dimensions, and fractures can form with slightly different intensity levels of each strain tensor. This causes for a slightly varied orientation, which causes the polymodal fracturing. This wide range of orientations in the past could have been confused with multi-modal fracturing, when in reality a single

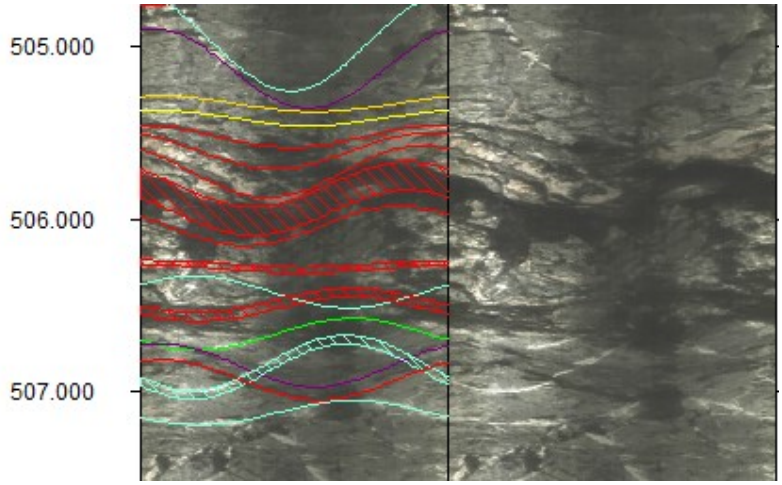

Figure 5.9: An example of a vein and an open fracture crossing, which suggests that they could have been formed at different times under varying mechanical stratigraphy

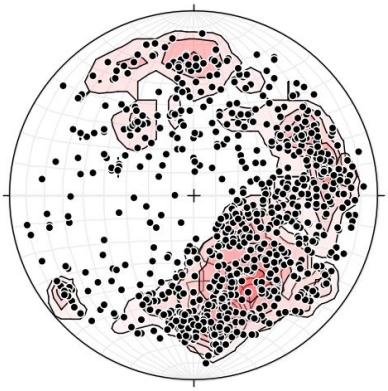

Figure 5.10: All open fractures

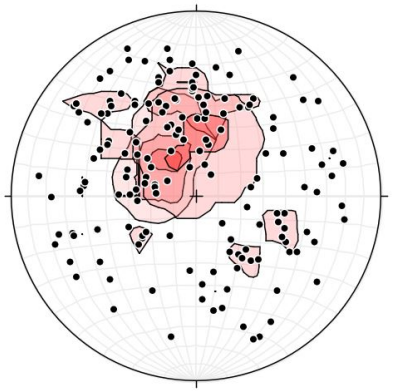

Figure 5.11: All veins

event can cause fractures to form in a polymodal like orientation (refer to figure 5.12)

This model will be populated in three dimensions and so the vertical fracture distribution needs to be extended laterally. In most cases the fault stress fields are used in order to make a prediction of the 3D stress field distributions, which in turn can help determine the fracture distribution patterns in the areas away from the well. In this case, the geological setting suggests that the fractures and the faults were created at different times in geological history. This can be verified

Formation	Open Fractures	Veins
Urgonien blanc et jaune	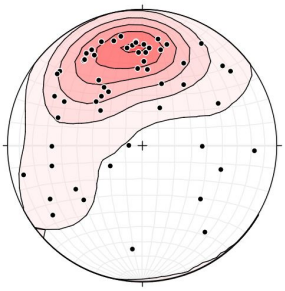	No veins identified
Pierre Jaune de Neuchatel	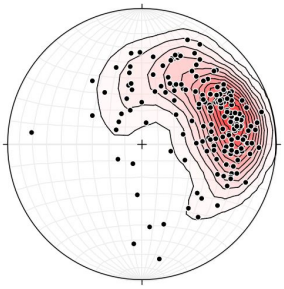	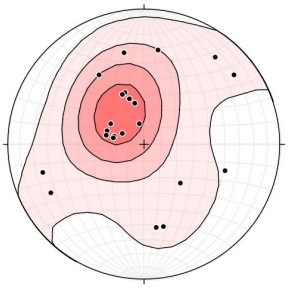
Marne d'Hauterive	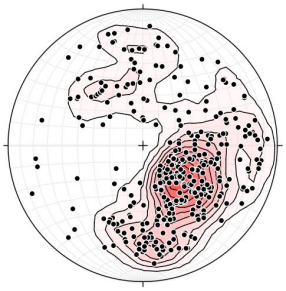	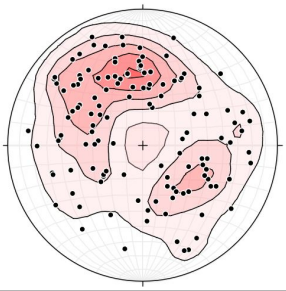
Complexe de marne et Calcaire Roux	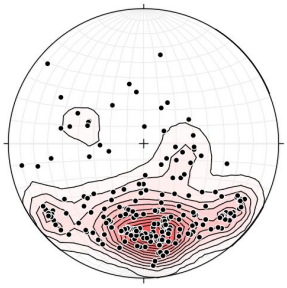	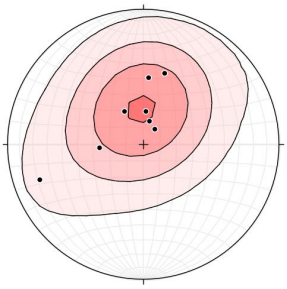
Chambotte inferieur	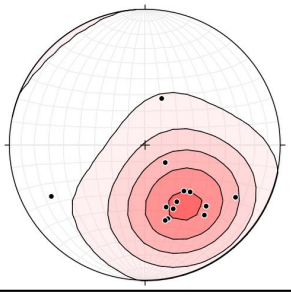	No veins identified

Table 5.2: Stereonet Plots by Formation separated into veins and open fractures

further using the fracture data, and matching it to the hypothesised stress regime of the faults. The lateral fracture distribution patterns will be further discussed in section 6.1.

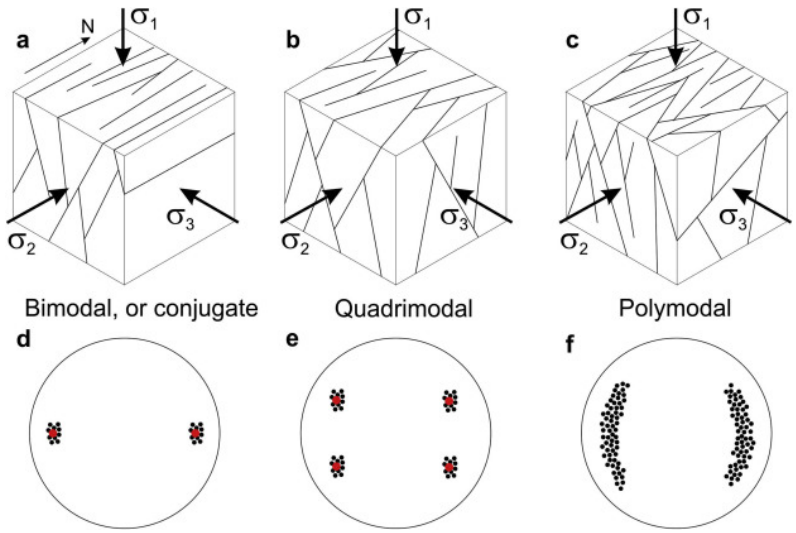

Figure 5.12: Polymodal fracturing in nature Healy et al. [2015]

Fracture Type	Total	Average Azimuth	Average Dip
Transverse Fracture	209	117.3	61.8
Non-Transverse Fracture	57	126.9	55.8
Transverse Vein	72	4.4	77.6
Non-Transverse Vein	30	314.2	68.8

Table 5.3: Overview of fractures from picking

5.6 STATIC PROPERTIES

The calculation of the Young's Modulus can be done in many ways with multiple equations this is because the calculation uses the ratio of stress and strain for that particular rock type. Since each rock formation has its own specific properties, there are many ratio combinations that can be applied. Since there is no core data available, the Young's Modulus can be approximated using well log data. This is what was done in the figure 5.13.

The reservoir is a carbonate reservoir made up mostly of limestone, bioclastic limestone, marly limestone and marl. Young's Modulus relationships with validity in limestone/carbonates would be ideal. The following table outlines the relevant relationships between various well log properties and E which were used to calculate the values in figure 5.13. As shown in the table, most of the Young's Modulus calculations give a very similar output, this is because they use the same variable, porosity. They have the same slopes, but the ratios used in each equation are slightly different. The two with the main differences are the equations which use the sonic velocity ratios.

The vertical distribution pattern of the fractures can be understood by looking at the mechanical stratigraphy and overlapping the fracture density patterns in order to assess whether there is a correlation between the two. This is done in order to identify whether the fractures in the borehole follow a mechanical stratigraphy, or if they have a different fracture stratigraphy. The main difference between these two options is the dynamic change of mechanical properties over time. What this means is that during the time of the formation of the fractures the formations had a slightly different mechanical stratigraphy to the present day mechanical rock properties (see section 4.3. Calculating the current deformational properties of the rock

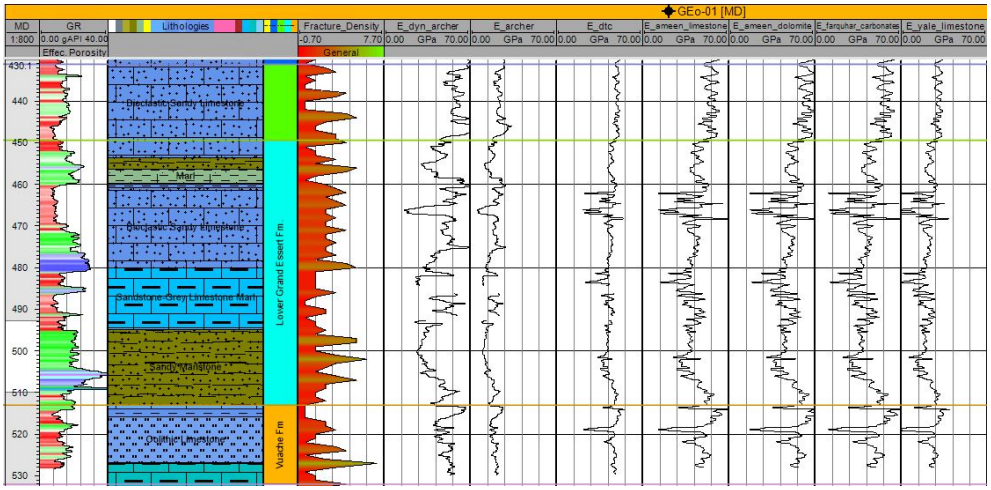

Figure 5.13: Young's Modulus Calculations

Relationship	Validity
$E = 86.094e^{(} - 5.43\phi)$	Limestone (Ghawar Field) *Ameen et al., 2009*
$E = 69.05e^{(} - 6.0\phi)$	Carbonates (UK North Sea) *Farquhar et al., 1994*
$E = 43.24 - 158.93^{\phi})$	Limestone (Kansas) *Yale and Jamieson 1994*
$E = 86.094e^{(} - 5.43\phi)$	Carbonates (Kansas) *Yale and Jamieson 1994*
$E = (UCS/13.8)^1/0.51$	Limestone *Chang et al., 2006*
$E = \rho Vs^2 * 3Vs^2 - 4Vc^2/Vc^2 - Vs^2$	Carbonates *Archer et al., 2012*
$E = 13474\rho * (3R - 4)/DTC * R * (R - 1))$	Carbonates *Gheibi et al., 2010*

Table 5.4: Different approaches for the calculation of the Young's Modulus Archer and Rasouli [2012]

(Young's Modulus) will help to differentiate if these fractures follow a mechanical stratigraphy or a fracture stratigraphy.

Young's Modulus measures the compressive and tensile strength of the rock in GPa which is indicative of how rigid a material is. This is why to classify the soft or stiffer layers of the reservoir the Young's Modulus is a good indication of how elastic a certain layer is. If a stiffer section corresponds to a high fracture density, then it can be said that the fracture density patterns match the current mechanical stratigraphy of the reservoir. There are multiple approaches that can be used to calculate the Young's Modulus, these approaches are based on relationships that are predetermined in a laboratory by experiments on different rock material.

The reservoir is a carbonate reservoir made up mostly of limestone, bioclastic limestone, marly limestone and marl. Young's Modulus relationships with validity in limestone/carbonates would be ideal. The following table outlines the relevant relationships between various well log properties and E. These are varying relationships between porosity, unified compressive strength and sonic velocities.The

resulting Young's Modulus are shown in figure Figure 5.13, using a range of cut offs between < 45 to $60E$, and > 25 to 14 gAPI (gamma ray), the distinguishing between soft and stiff layers was created and compared to the fracture density log to determine which cut offs would be ideal to determine the varying 'k' layers for the dfn generator. The cut off used was; $20gAPI > stiff > 54E$.

This cut off value does however classify the two large marl sections (453-460m and 494-512m) as soft layers, which means that fractures would not be modelled in these areas. However, the OBI shows that the upper part of the marl section between 494-504m is highly fractured. This suggests that the fracture pattern does not match the current mechanical stratigraphy. If this is the case, then the fracture model will have to rely on the fracture stratigraphy, where only the OBI can be used as input data. This means that the fracture patterns in the reservoir, because they were formed a long time ago, will no longer follow the patterns of the current mechanical stratigraphy (refer to flow diagram in figure 5.14. This implies the the mechanical stratigraphy has changed over time and that the mechanical stratigraphy that was present during the formation of the fractures is no longer relevant.

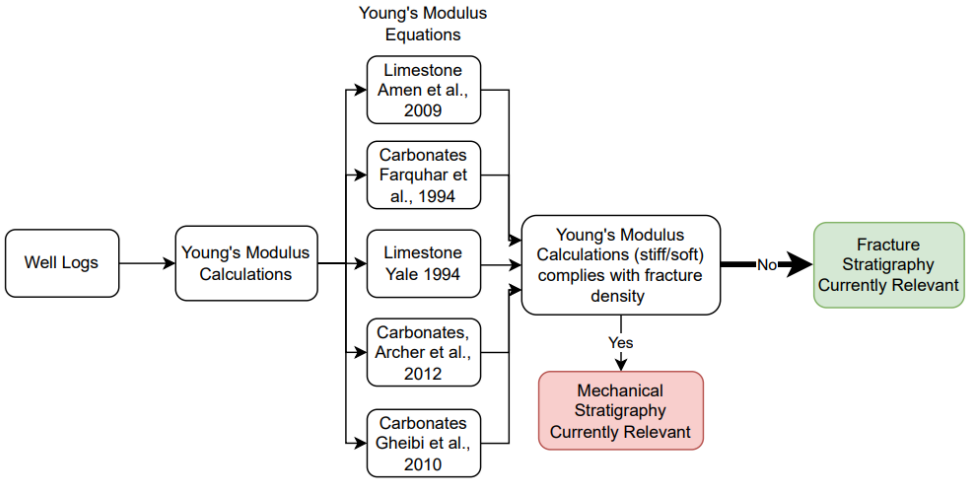

Figure 5.14: Flow Diagram for workflow in determining the relevance of Fracture stratigraphy

As shown in 5.15, the sections in the marks are the bedding which have consistently high peaks. The bioclastic sandy limestone appears above and below the marl, but at the depth of 433 to 455m there seems to be a highly varying fracture density. At the depth of 460 to 480m there seems to be little fracture density. This could mean that this area of the well could be inconsistent with the rest, or that the upper biolcastic sandy limestone package has (or had) a different mechanical stratigraphy. Using the fracture stratigraphy to populate the model this initial differentiation can help determine which k-layers to group together and which to omit. The k-layer concept will be further explained in the next section.

5.7 STRUCTURAL MODEL

The 3D grid that is created for the simulation consists of 5 horizons and 4 sections; Urgonien blanc et jaune (top), Pierre Jaune de Nauchatel (top), Marne d'Hauterive (top), Complexe de marne and Calcaire Roux (top) and Chambotte inferieur (bottom). The boundaries of the grid are drawn around the 4x4km area of these surfaces. The grid contains 68 grid cells in the i direction and 70 cells in the j directions. The number of k grid cells (k layers) is 55 which will then later be converted into stratigraphic sections in accordance with the parameters of the fracture growth model.

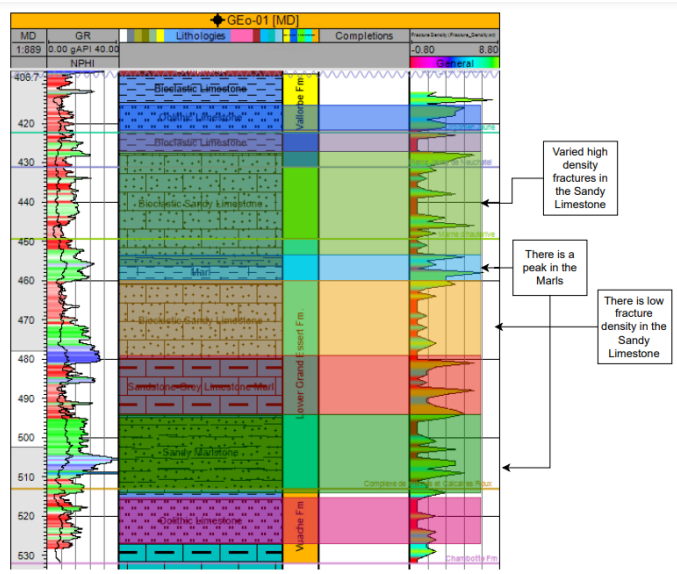

Figure 5.15: Assessing fracture distribution; Lithology is shown in the wide column in the middle, and seems to roughly correspond with the fracture density readings on the right.

There are 55 k layers in the structural model since the reservoir cross section is roughly 120m in thickness from 413m to 533m measured depth. The first formation; Urgonien blanc et jaune to Pierre Jaune de Nauchatel will be split by 5 layers, the next by 10, then 30 and then 10, this results in k-layers that are roughly 2m thick. This can be seen in figure 5.16 where the 3D grid has been separated into 2.2m k layers. These will then be redefined into groups of k layers using the fracture density curve. This refers back to the stress shadow explanation in section4.3.

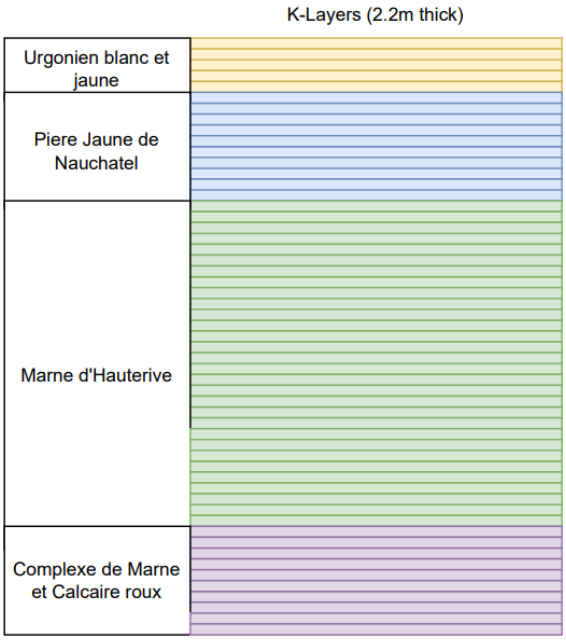

Figure 5.16: k Layers per formation

The grouping of these k layers will determine the intensity of the fractures in a certain modelled layer. The more k layers grouped together, the less dense the fracture network will be. This is because of the way the stress shadowing works,

with a larger k layer, there will be a larger bed for fractures to be confined to and the less fractures will form per area.

The importance of the *k* layer in the G-DFN model will be the density control. The DFN generator controls the number of fractures per area by the size of the *k* layer. This means that a G-DFN layer modelled with 3 *k* layers will have a lower fracture density than a DFN layer modelled with just a single *k* layer Welch et al. [2022]. This will be discussed further in section 6.2.

The benefit of being able to group this 3D grid into k layers is that it is possible to run the G-DFN for a full reservoir model and omit some layers that have no fractures. In an interval which shows one or two fractures per meter, the G-DFN could omit these interval as fracture-less intervals. This could be cross referenced and attributed to layers that are after of did not develop any fractures.

6 MODELLING

In the previous data section key choices for the geomechanical fracture growth model were determined. Fracture stratigraphy instead of mechanical stratigraphy was chosen to model the vertical variation of fractures because the fracture density data did not match the rigidity of the rock mass. This choice will have an effect on the building of the model in the grouping of the k layers (see section 5.7. Using the fracture density graph obtained through the fracture picking mechanical layers for the G-DFN growth model was created (see figure 2)

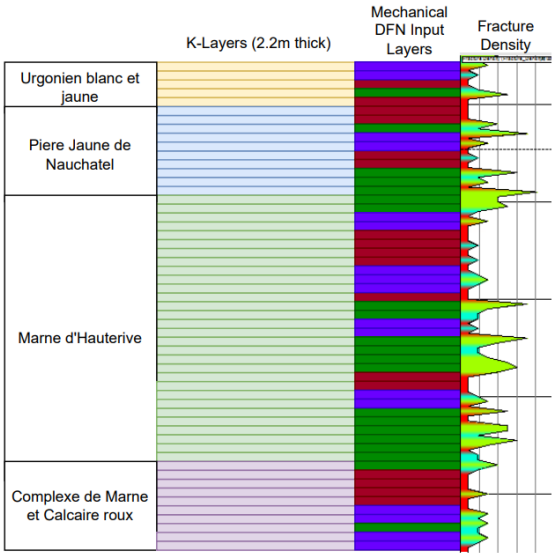

Figure 6.1: Combined k layers to control for density using the stress shadow and disregarding layers with low fracture density. The blue colors are for low fracture density areas where stress shadow effect will be used by increasing the size using multiple k layers, green represents high fracture density areas where a single k layer will be used and red layers will not be modelled

Running the fracture growth model as explained in section 4.3 will start with small micro fractures and then increase in size as the time of the model elapses turning in to macro fractures of a rectangular shape. Changing the number of sets will increase the fracture modes (increase variation in fracture orientation). An increased number of fracture sets also significantly increases the number intensity of fractures in the grid cell.

This sets determine the number of fractures that will propagate from one single point in the model. In this case the number of sets used was two, due to the fact that in the fracture data the majority of the fractures favoured normal fractures. As shown in figure 6.2, the image 6.2a shows a maximum of two branches from a point, while 6.2b shows four and 6.2c shows six. Sets of 6 are mainly used in more advanced strike-slip fracture networks. Since the data from the OBI shown in table 5.2, shows that the most part of the fractures show a normal regime, the number of sets for the purposes of this model will be two.

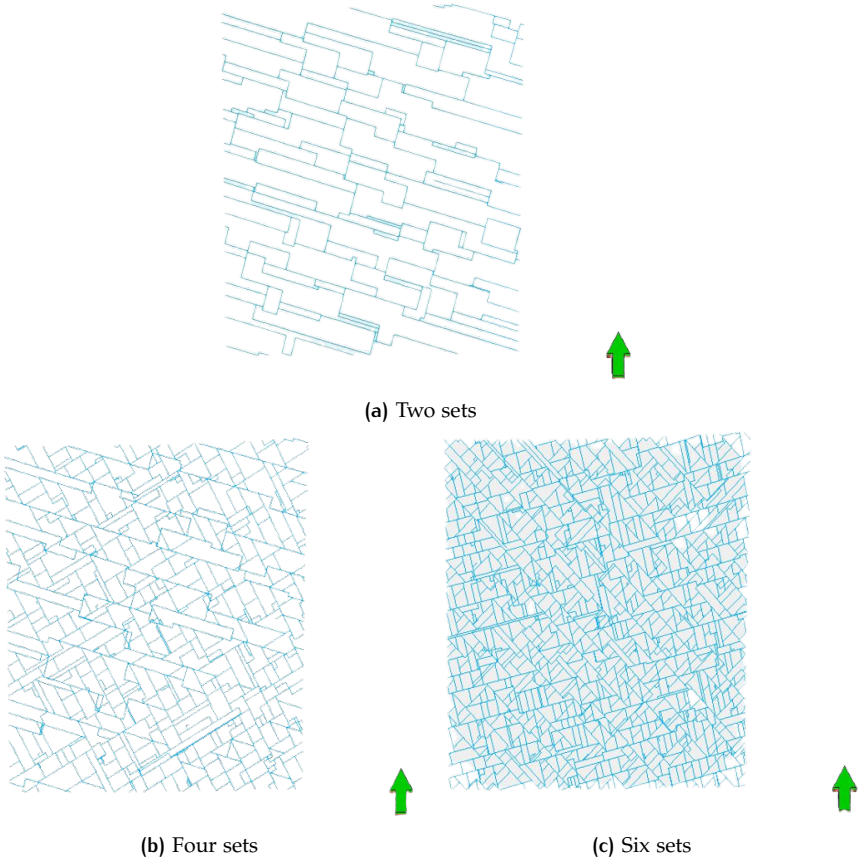

(a) Two sets

(b) Four sets

(c) Six sets

Figure 6.2: Growth patterns for various fracture set combinations for the DFN Generator

6.1 PALEO-TECTONIC STRESS CALCULATION

The paleo-tectonic stress calculations are a crucial part for accurate model development, these variables make up the core of the geomechanical fracture growth model approach. The paleo-stress is a calculation of the stress regimes that were active during formation of the mechanical deformity. This can be done for any mechanical discontinuity, but it has mainly been done for faults and folds. In this study, there is a mismatch between the fracture data and the fault data. A suggested approach by Maerten et al. [2016] recommends the method of trial and error. In the methodology by Maerten et al. [2016] they use a programme called Nash Point which runs 50,000 simulations within 2 minutes outputting the optimal scenario of faults with respects to the fracture data provided.

The paleo-stress inversion technique is a process within petrel that uses the orientation and dip/strike of faults to calculate the strain distribution along across the grid (Maerten et al. [2016]). This step calculates the probability of the different types of stress regimes at varying orientations of σH outputting a graph shown in Figure C.1. The graph shows the confidence intervals on the color legend on the right and the probability of the stress regime being a Normal, Strike slip or Reverse.

Another way to calculate stain data that does not take into consideration the faults is to use the curvature values for the unconformities of the horizons. This can be easily calculated in petrel using the operations commands within the each surface. The max and min curvature can be used to make a rough estimate for the min and max strain rate (respectively).

The azimuth of max curvature can be used as an input for the horizontal strain. The method using surface curvature is most commonly used in situations where

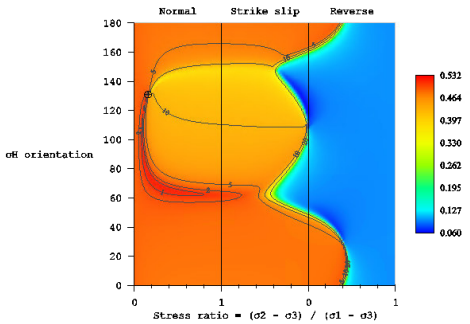

Figure 6.3: Paleo stress inversion back calculated through Petrel plug in

most of the fracturing can be attributed to folding. If the fracturing is not attributed to the faulting, as it is in this case, calculating the stress using the paleo-tectonic stress inversion technique could corrupt the fracture data. Therefore a similar method to the one used in Maerten et al. [2016] will be used.

The graphs in Appendix C.1 show the probability of the stress regime calculated though Petrel using fault and fracture data. There is a small black circle with a small cross on it, this represents the regime that is most likely under that scenario. From these scenarios using both the fracture data and the fault data is was very to determine one single optimal stress regime. The fractures were indicating normal, while the faults were indicating strike-slip, running just the faults creates paleo-stress charts which highly favour the reverse stress regime, however when integrated with fracture data the model cannot converge properly. Through some trial runs using less faults that were further away from the well a scenario was created that fits the stress regime by 53%. This is shown in figure 6.3 where the preferred stress regime is normal, the stress ratio is 0.16, the orientation is 131 degrees, with a sigmaH of 1.2E06 bar, sigmah of 7E05 bar, sigmaV of 1.87E06 bar.

6.2 GEOMECHANICAL FRACTURE GROWTH MODELLING

The geomechanical approach by Welch et al. [2022] is a powerful tool that is able to take petrel grid with properties (Young's Modulus, Poissons Ratio, friction coefficient, etc.) and use these values to create a G-DFN with varying fracture densities and fracture sets. The G-DFN will only use the stiff layers to generate fractures assuming the fractures in the softer layers do not form in relevant quantities to model for fluid flow upscaling.

The G-DFN uses the maximum horizontal strain, minimum horizontal strain and minimum horizontal strain azimuth distribution as the main input settings to create the fracture growth model. Mechanical properties such as Poisson's ratio and Young's Modulus can be toggled either given a single value for the full grid, or by using a 3D property grid. For the purposes of this study, the default value will be used since the calculated mechanical properties are not accurate for fracture modelling of this reservoir. The input parameters can be seen in table **??**. The stress shadow can be toggled on or off, if toggled off the stress will be evenly distributed over the entire grid. If toggled on, then there will be areas in which stress values are lower due to proximity to high stress area.

With reference to the max and min strain rate, the DFN model will output varying fracture densities increasing in areas with high strain values (i.e. near fault zones and/or areas with high curvature) and low fracture densities in ares with less strain (i.e. away from faults and/or ares with low curvature).

7 RESULTS

7.1 FRACTURE NETWORK

The output of the fracture growth model is a combination of layers made up a grouping of k-layers with individual elongated rectangular fractures (figure 7.1). These individual layers represent the bed confining fractures. The G-DFN comes out layer by layer, each undergoing its own fracture growth phases. The fractures in the layers can interact with the top and bottom layer if there is no space in between. Permeability in the k direction is usually similar to the permeability in the i or j directions. This k directional permeability is calculated independently from the other layers in proximity. Each layer when created is isolated from the other. The connectivity comes when upscaling the properties for fluid flow simulations.

Where the modelling process omitted a layer (between the k-layers due to low fracture density) there could result in a barrier to flow. This is one limitations of this method, if the model is upscaled, then this could cause problems during fluid flow simulation. In reality the connectedness of the reservoir is heterogeneous, in this case full sectors of the reservoir could be close off. From the side view shown in figure 7.3 as well as investigations layer by layer show that the fracture intensity control variable of strain has a higher effect on increasing the density of the fractures in the growth model.

Figure 7.5 shows a fracture density pattern not controlled by the faults, as the DFN layer in this figure has faults dipping towards the NE-SW. If the DFN were based on the faults, there would be slightly higher density fracture areas along the fault lines or the absence of any fractures depending on the stress shadow of the fault. Instead, in this model based on the fractures, which shows a similar density of fractures along the full grid cell. This can be seen from 7.2. Here there is almost a uniform patter of fracture orientation and dip until the discontinuity on the northeast. This discontinuity represents the fault used to predict the ideal stress regime conditions for the fractures.

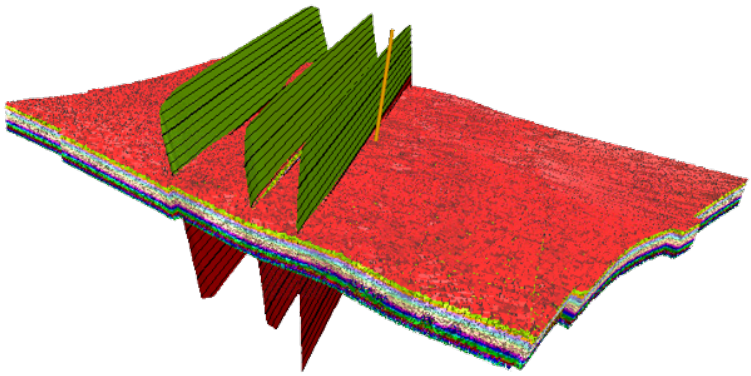

Figure 7.1: Overview of DFN with strain calculated from fracture insitu stress calculation

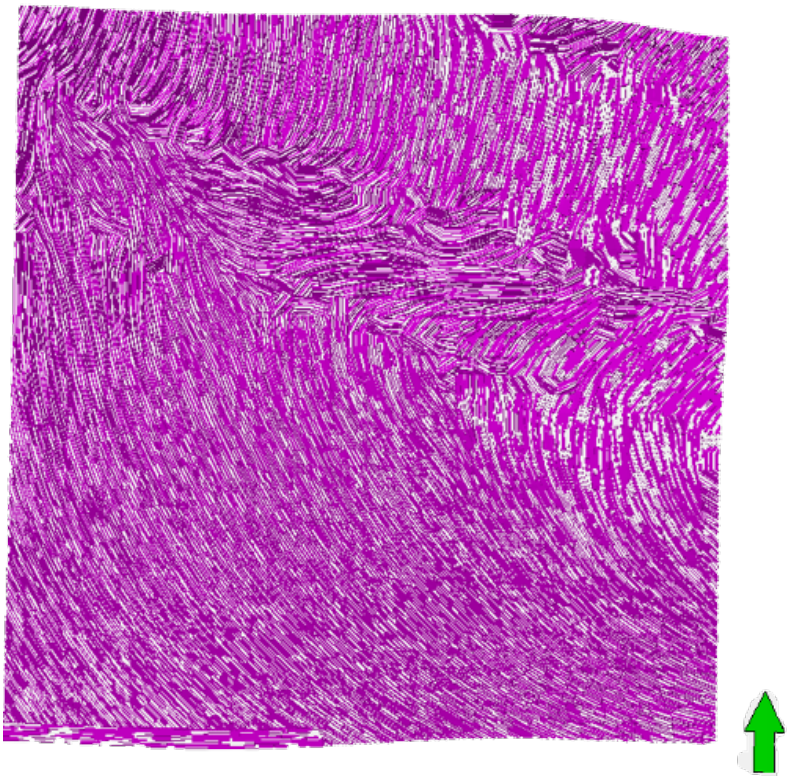

Figure 7.2: Top view of the behaviour of the fractures when not controlled by fault strain

Figure 7.2 shows the general pattern of the fracture growth model, referring back to section 5.4, most of the fractures are oriented towards 117 degrees with a dip of roughly 60 degrees. Using 2 sets during the fracture growth propagation, the average dip of these fractures is also 60 degrees. Looking at the figure 7.2 it also seems that the orientation of these fractures is roughly 120 degrees. A conclusion from this is that the geomechanical fracture growth model has the capabilities to deliver seemingly accurate results. A continuation process of the validation of this step would be to upscale and use well testing data for validation of a fluid flow model.

This fracture model with the output fractures shown in figure 7.2 shows the expected orientation of fractures closer to the well in the middle of the DFN model. Due to the fact that it was difficult to create a stress inversion calculation without faults, two of the faults were used. The error margins for the fractures around these fault locations are very high due to the fact that these orientation are unknown. Focusing just around the fractures in the middle section closer to the well, correspond with the orientations in the fracture data as shown in table 5.2.

The fracture density controls provided by the k-layers through stress shadowing are not immediately apparent. What can be seen is that there are large (taller) fractures being formed in the blocks with multiple k layers. Due to stress shadowing, because of the increased surface area of the individual fracture, there is less space for other fractures to form due to the proximity. This is why larger layers will have slightly less dense fracture population. From the side view shown in figure 7.3 it is seen that the fracture intensity control of strain (E1 and E3) have a higher effect on increasing the density of the fractures in the growth model. An example of this is seen in figure 7.4 where the curvature of the layer decreases and there are significantly more fractures that have populated the area.

The result of the geomechanical approach fracture growth model with a curvature calculation shows the influence of horizon max and min curvature on the intensity of fractures. It can be seen in figure 7.4 that the fractures intensify in areas

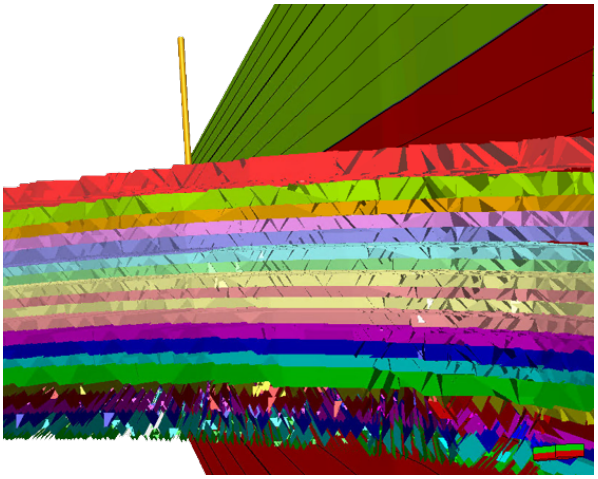

Figure 7.3: Zoomed in side of DFN from fracture insitu stress calculation

of high curvatures and become sparse in areas of low curvature. This method is best used for a scenario in which the fractures would be attributed to the folding of the Jura mountains in the NW. If this folding were to have fractures the rock matrix, then this would have been an interesting approach.

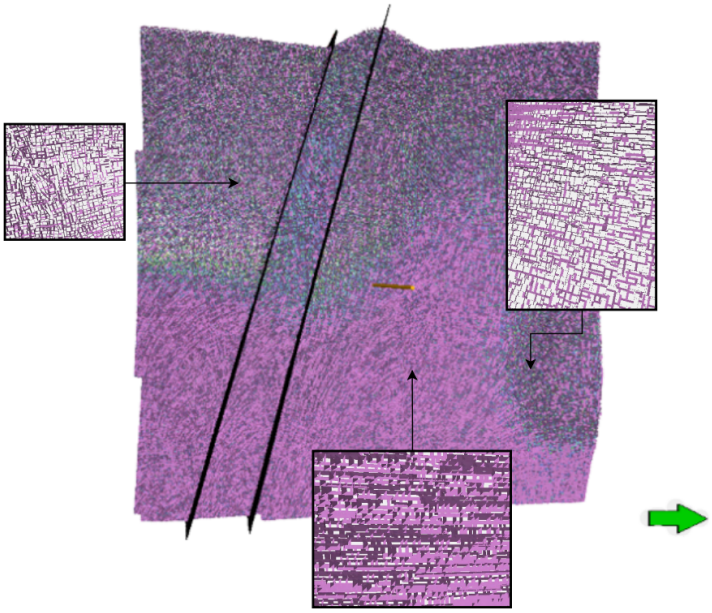

Figure 7.4: Top view of DFN from strain calculated from curvature

The close up of the DFN in figure 7.5 shows the interaction between the DFN populated fractures and the faults that were not used in calculating the strain. This would ideally be the situation when using the paleo-tectonic stress inversion tool. However, the reality is much more like figure 7.2 where the fractures populated in the model agglomerate around the fracture. This aspect of the model is a major limitation and should be addressed if anyone takes this further.

Figure 7.3 shows the side of the fracture orientations of the model, and here you can see that the fractures have a slight rotating pattern seen similarly to the rotational pattern through depth of the figures in table 5.2. This is a huge generalisation of the reservoir area, because the only point of data available is from the middle of the well and therefore the margins or error in this model are major. The advantage of using this fracture growth model is that the fractures seen in one sin-

gle point can be regrown under the same pressure conditions and have the density and orientation be some what similar to the actual situation in the subsurface. For this to have relevance the GEO-01 well would have to be an example of the general fracture patterns within the 2x2km radius.

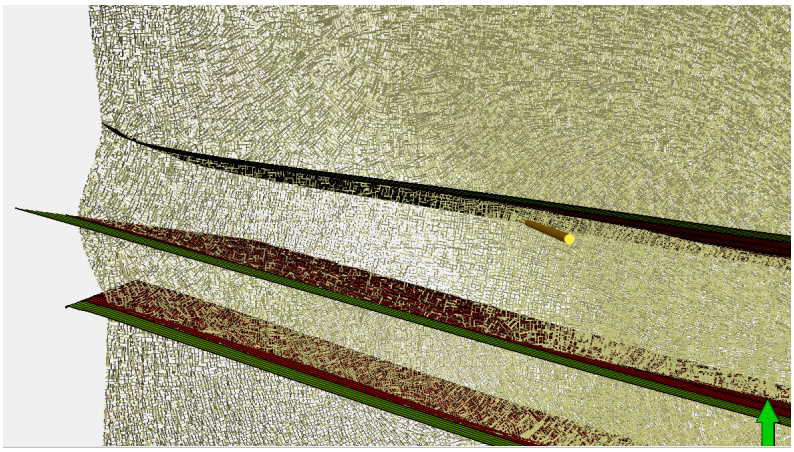

Figure 7.5: Close up of DFN without any fault influence (taken from curvature output)

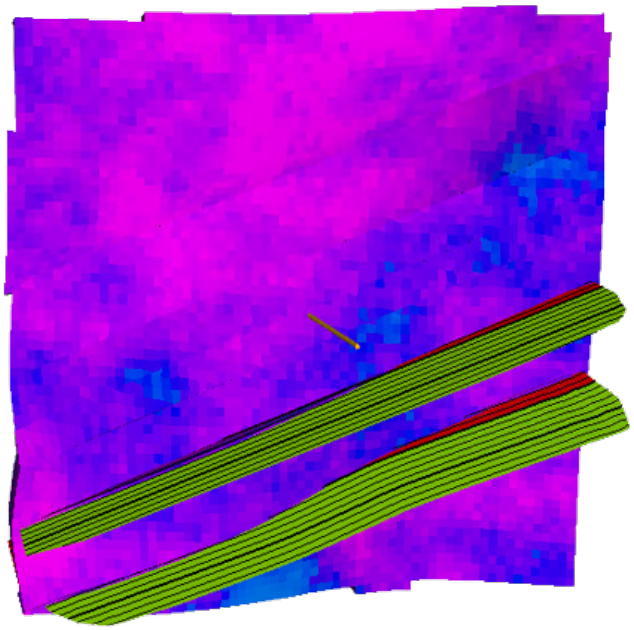

Figure 7.6: Top view of permeability in the k direction from the fracture insitu stress calculations

The fracture growth model not only outputs a DFN but also created permeability coefficients in various different directions. These parameters can be upscaled with the matrix permeability to create a grid property that can be used in dynamic simulations and fluid flow. This is where the value truly comes in with these generated DFN models as they can be a huge gap filler in exploration projects, and hopefully validated later using well tests.

In previous sections there was a lot of mention of mechanical stratigraphy versus fracture stratigraphy. From the evidence collected in this study it is apparent that there are some changes in the mechanical stratigraphy due to the differences in fracture density and the mechanical properties of the rock. This means that there

could be two sets of fractures that were formed under different circumstances. For this scenario, a suggestion would be to superimpose two G-DFN runs on top of each other; i.e. by adding their permeability grid properties together. This would create a grid that takes into account both fracture sets during two different stress events.

In previous sections there was a lot of mention of mechanical stratigraphy versus fracture stratigraphy. From the evidence collected in this study it is apparent that there are some changes in the mechanical stratigraphy due to the differences in fracture density and the mechanical properties of the rock. This means that there could be two sets of fractures that were formed under different circumstances. For this scenario, a suggestion would be to superimpose two G-DFN runs on top of each other; i.e. by adding their permeability grid properties together. This would create a grid property ready for upscaling that takes into account both fracture sets during two different stress events.

8 DISCUSSION

An advantage of having this fracture growth model is ideally this method would be able to predict the fracture network in a reservoir with limited access to data. The requirements are that the limited access to data gives a somewhat accurate understanding of the stress regime of the area during fracture formation. If this is known, then the DFN model would be able to run through time-steps calculating the orientation, density and positioning of the fractures based on a mechanical stress based approach. This would work well in areas where the fracture growth could have resulted from folding, since the curvature of the horizons can also help create a stress map. The issue with this Geneva basin case study was that there was no data on the fault orientation. This was a major handicap in calculation the stress field of the fractures. It was also found that the fracture dip angle did not match the original hypothesis that the fault was as strike slip fault. This could mean that the fractures and the fault were created at different times.

8.1 PALEO-STRESS CALCULATION

The paleo-stress calculation is one of the most crucial pieces of this model. The paleo-stress calculation determines the lateral distribution of fractures across the study area. This plays a huge role in the prediction of fluid flow pathways during dynamic simulation. The paleo stress inversion technique in this study is the weakest part of the model. This could have been improved drastically using other methods for strain calculation such as WinTensor [Delvaux, 2011].

The stress calculations for the inputs of the fracture growth model could have been tuned to recreate the insitu stress regime. A focus on the geological history and using a combination of Petrel and the Elastic theory equation could have resulted in paleo-tectonic stress calculation with stronger arguments. This is a limitation to this model, but also a limitation to the tools offered in Petrel since it is not possible to create a paleo-tectonic stress calculation without the presence of faults. If events in a geological history did not happen at the same time, there should be a possibility to separate the two events of deformation.

The geomechanical modelling tool focuses on decreasing uncertainties, and the fracture growth model itself can decrease uncertainties during exploration, but would work better in an area where there has not been so much tectonic activity and where the fracture data orientation and dip would comply with the present faults in the region. An option for this specific case study could be to do a further investigation into

8.2 DIFFERENCE BETWEEN OTHER APPROACHES

The most recent G-DFN created very similarly to the process steps took in this study was done by Alhamad [2020], this takes into account the different fault models. The focus of the paleo-tectonic calculation and strongly links faults identified in the seismic with the fracture data. The mechanical stratigraphy of the DFN generated

is based on a mechanical stratigraphy that does not take into account the fracture density.

The fracture growth model as mentioned in 5 uses the thickness of the layers to control the fracture density, fracture density is an important parameter when modelling fractures because this can have an affect on the permeability of a region of the reservoir. This is the main difference between the network model that was created in this research paper. Building on the work that was done on the mechanical units by Alhamad [2020], this research was able to take a different perspective to modelling the DFN from a fracture stratigraphic profile versus a mechanical separations.

There is a high discrepancy as to the interpretations of the faults data, with the interest accumulating withing the exploratory phases of the Geneva basin project there is opportunity to further investigate the fracture data focusing on the cross-cutting relationships between fractures or if there could be some stylolites.

8.3 LIMITATIONS

The unknown orientation of the faults are a major limitation due to the fact that this creates a lot of problems with finding the insitu stresses. There are plans for further exploration in this area, which would benefit from some insights into seismic data to better locate the surrounding faults. If this is not an option, then once there are well data available, it is possible to check multiple fault orientation hypothesis and trial them to understand which works best. This was takes longer but it is significantly cheaper.

Due to the fact that there is a large area with just one well borehole to use to classify the entirety of the 3D model, small errors can compound quickly. Even if the fracture picking analysis from the OBI was accurate, there is no guarantee that this fracture density pattern can represent the rest of the area. This issue can be solved by creating dynamic simulations along side flow data from the well to understand if the flow patterns match the simulation. Having data for another well would also be beneficial in validating results for fracture density. The Geneva basin project has drilled a second well; GEO-02 in the proximity of the GEO-01 well. Using this data as validation would be a beneficial continuation of this project's research.

The tools used to calculate the paleo-tectonic stress require that a fault geometry be present in the calculation which made it difficult to get results based only on the fracture data. This limitation could be explored further by using software to investigate if there is a large difference between using fracture data as input without any fault data. This would help to confirm the assumption made in this thesis about the different formation age of the fractures versus the faults in this area.

Using curvature data alone to calculate the fracture density within a layer may not do a very accurate estimation as the curvature of the layers would have changed since formation. This therefore is an inaccurate way of representing the horizontal distribution of fracture patterns. The curvature for this case is also difficult to validate since there are only two perpendicular seismic lines. Estimating curvature from the surfaces create a large error margin.

It could be interesting to delve deeper into the differences between these two approaches to see what are the effects of varying the k layers and if there is a big difference on the distributed fracture density. It would be interesting to see one of these models pushed towards a dynamic simulation, this would then give better understanding towards the pitfalls and strengths of this approach.

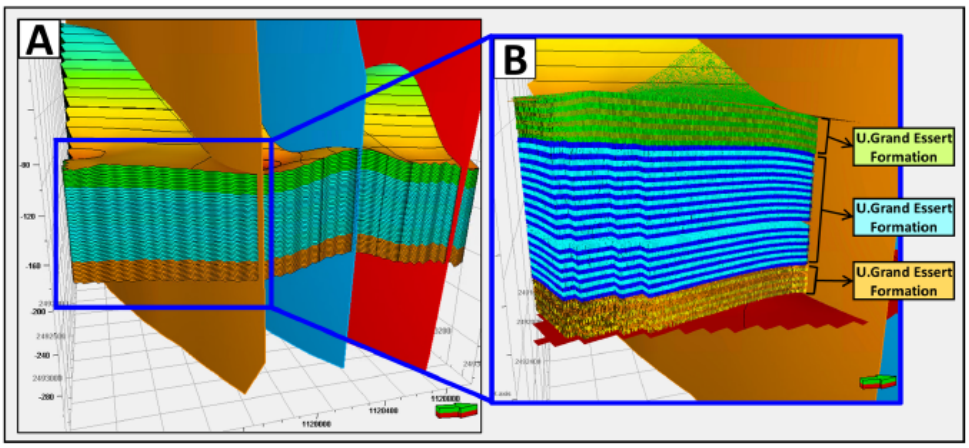

Figure 8.1: Fracture Network by Alhamad [2020] showing the DFN generated with k layers that are evenly spaced out and a different fault model

8.4 DFN CRITICISM

The main handicap in the modelling of this discrete fracture network is the fact that there is only one control point. With a second well, the horizontal data predictions would be a lot more accurate. The current fracture density and orientations are solely based on one vertical well section. This means that the horizontal fracture distribution and orientations are arbitrary and based on a predicted tectonic stress regime.

The goal behind creating a G-DFN model is to be able to better predict the flow regime within a reservoir to be able to optimise the placement of doublets for production. This would be able to help create a better understanding of the movements of the water flow within the context of a geothermal doublet. However, even if we make a very accurate model that fits the current data, the limitation here is the lack of data, and affects the precision of the model created.

In order to advance the precision of the model, a second well is needed with OBI data to be able to use a second data point with which to compare and refine the current fracture growth model model. This new data would be able to contribute to the paleo-stress inversion techniques used in order to predict a precise orientation and magnitude. Which are the main inputs for the fracture growth model calculations in order to create fractures that are closely related to the subsurface by using more control points.

Using one well control point makes it so that the vertical horizon of fractures is known. This helps with finding layers of the reservoir that may be more fractured than others. However, it does not help with determining flow direction since the data used to determine a horizontal flow direction is vertical data. There is no way of knowing if the fractures will switch orientations and create a flow barrier instead of a fluid flow pathway.

A recommendation to take this analysis further is to have a look at the different possible orientations of the fractures and run a DFN to check if these orientations would match the orientations of the fractures instead of an unnatural pattern shown in figure 7.2. This would help in making an informed decision as to the hypothesis on fault orientation. This could then further be validated with the continuation of seismic exploration in the area. If there are no new seismic lines, this approach could also be further validated using a fluid flow simulation model and well tests to compare.

9 CONCLUSION AND RECOMMENDATIONS

The Geneva basin is an area of very active geological history, making for an interesting case study. This project would benefit from more time looking into the origin of the fractures. Once the origin of the fractures is known, the paleo-tectonic stress calculations would become simpler, and the model more precise. This is assuming there there is a better way to exclude faults in the stress calculations through petrel. An alternative is manual calculation given a certain boundary constraints and parameter create a 3D property grid with customised E1 and E3.

A thorough investigation into the fractures was necessary and created space for new questions. It is extremely useful to have fracture imaging data to rely on, but even being able to see the fractures themselves can create dispute between researchers. Between the three authors working with the raw OBI data, each one had their own interpretation of the results.

The fracture growth model has the ability to handle fracture specific data, but there is a need to increase the capacity of supporting tools to be able to create data that is reliable. Without support for the choices made during data collection, there is very little value that the output model can bring.

9.1 RECOMMENDATIONS FOR FURTHER RESEARCH

Some possibilities to take this research further, could be to explore the seismicity potential risk, using a finite solver such as OpenGeoSys (OGS). Seeing as this geothermal doublet will be drilling in the city center of Geneva, the potential risks of seismicity due to fracking, or EGS could be explored. This process could entail creating a mesh like environment of the area and (9.1).

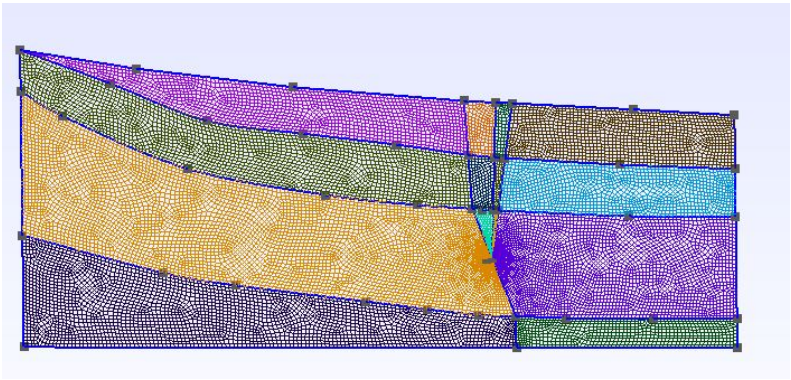

Figure 9.1: Final fixed Mesh for NW-SE oriented faults

Another possibility for extension of this research very relevant for the current stage of the Geneva project is to run a dynamic model using DARTS and use field data to validate the DFN results with regards to fluid flow pathways and permeability. This would help with insights into whether the assumptions made in this thesis were accurate enough to be able to predict some mechanisms of the subsurface. A dynamic simulation of the DFN would require the up-scaling of fracture properties

to permeability using the Carmen-Kozeny equation. This uses the aperture of a single fracture and converts this value to permeability. This permeability value can then be added onto the rock permeability and exported to DARTS for fluid flow simulations.

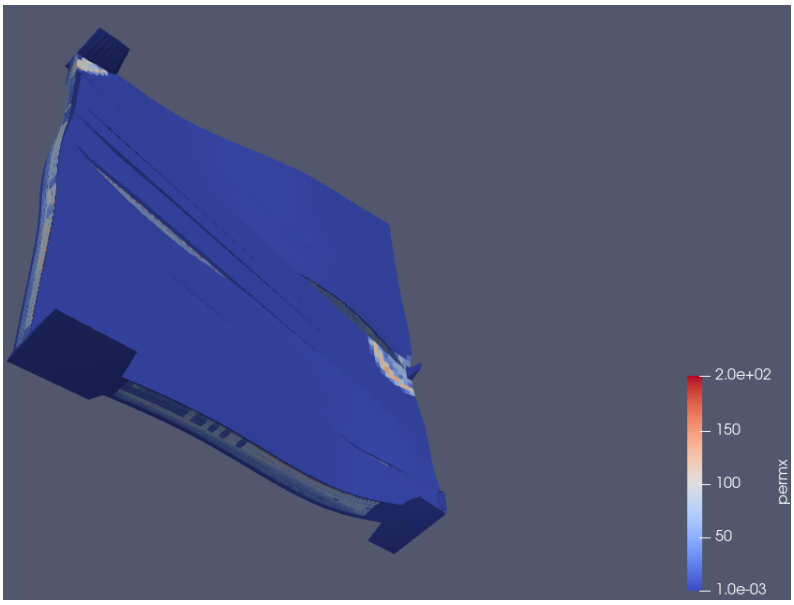

Figure 9.2: DARTS permeability model

BIBLIOGRAPHY

Alhamad, M. (2020). Fracture network prediction in the geneva basin: A geotheramal case study. *Master Thesis*, pages 1–70.

Archer, S. and Rasouli, V. (2012). A log based analysis to estimate mechanical properties and in-situ stresses in a shale gas well in north perth basin. *WIT Transactions on Engineering Sciences*, 81:163–175.

Barton, N., Bandis, S., and Bakhtor, K. (1985). Strength, deformation and conductivity coupling in rock joints. *International Journal of Rock Mechanics and Mining Sciences and Geomechanic*, 22:121–140.

Brown, S. and Scholtz, C. (1985). Broad bandwidth study of the topography of natural rock surfaces. *Journal of Geophysical Research*, 90:575–582.

Bruna, P., Prabhakaran, R., Bertotti, G., Straubhaar, J., Plateaux, R., Maerten, L., Mariethoz, G., and Meda, M. (2019a). The mps-based fracture network simulation method: Application to subsurface domain. *81st EAGE Conference and Exhibition 2019*, 1:1–5.

Bruna, P., Straubhaar, J., Prabhakaran, R., Bertotti, G., Bisdom, K., Marietho, G., and Meda, M. (2019b). A new methodology to train fracture network simulation using multiple-point statistics. *Solid Earth*, 10:537–559.

Buijze, L., van Bijsterveldt, L., Cremer, H., Paap, b., Veldkamp, H., Wassing, B., van Wees, J., van Yperen, G., ter Heege, J., and Jaarsma, B. (2020). Review of induced seismicity in geothermal systems worldwide and implication for geothermal systems in the netherlands. *Netherlands Journal of Geosciences*, 98:doi:10.1017/njg.2019.6.

Chablais, J. and Rusillon, E. (2020). *Litholog de forage - Litholog Report (LLR)*. GEothermie 2020, Geneva, Switzerland.

Chandrasekaram, C. and Bundschuh, J. (2008). *Low Enthalpy Geothermal Resources for Power Generation*. CRC Press, Leiden, Netherlands.

Charollais, J., Wernil, R., Moscariello, A., Metzger, J., Busnardo, R., Clavel, R., Conrad, M., Davaud, E., Saint Martin, M., and Weidmann, M. (2013). Presentation d'une nouvelle carte geologiues du vuache et du mont de musieges (haute-savoie, france). *Stratigraphie et tectonique*, 66:1–64.

Clerc, N., Rusillon, E., Cardello, L., Moscariello, A., and Renard, P. (2016). Structural modeling of the geneva basin for geothermal ressource assessment. *Swiss Geosciences Meeting, Geneva*, 14:10.

Delvaux, D. (2011). Win-tensor, an interactive computer program for fracture analysis and crustal stress reconstruction. *EGU General Assembly*.

DiPippo, R. (2012). *Geothermal Power Plants: Principles, Applications, Case Studies and Environmental Impact*. Butterworth-Heinmann, Oxford, UK.

Do Couto, D., Moscariello, A., Daher, S., Littke, R., and Philipp, W. (2021). Origins of hydrocarbons in the geneva basin: insights from oil, gas and source organic geochemistry. *Swiss Journal of Geosciences*, 11:114.

Floros, I., Tserpes, K., and Lobel, T. (2015). Mode-i, mode-ii and mixed-mode i+ii fracture behavior of composite bonded joints: Experimental characterization and numerical simulation. *Composites Part B: Engineering*, 78:459–468.

Gupta, H. and Chadha, R. (1995). *Induced Seismicity*. Birkhauser Basel, Hyderabad, India.

Haring, M., Schanz, U., Lander, F., and Dyer, B. (2008). Characterization of the basel 1 enhanced geothermal system. *Geothermics*, 37:469–495.

Healy, D., Blenkinsop, T., Timms, N., and Meredith, P. (2015). Polymodal faulting: Time for a new angle on shear failure. *Journal of structural Geology*, 80:197–213.

Helgeson, D. and Aydin, A. (1991). Characteristics of joint propagation across layer interfaces in sedimentary rocks. *Journal of Structural Geology*, 13:897–911.

Hoek, E., Kaiser, P., and Bawden, W. (1995). *Support of underground excavations in hard rock*. Mining Research Directorate and Universities Research Incentive Fund, Vancouver, Canada.

Huang, X., Xu, M., Zhang, Z., and Lei, Q. (2020). Characterizing stress variability within granular samples upon liquefaction. *Computers and Geotechnics*, 127:online.

Karimi-Fard, M., Durlofsky, L., and Aziz, K. (2004). An efficient discrete-fracture model applicable for general-purpose reservoir simulators. *SPE*, 9:227–236.

Koumrouyan, M. (2019). Geomechanical characterisation of geothermal exploration borehole. *Master Thesis*, pages 1–93.

LearningGeology (2015). Learning geology: Fracture types, http://geologylearn.blogspot.com/2015 /08/types-of-fractures.html.

Lei, Q., Latham, J., and Tsang., C. (2017). The use of discrete fracture networks for modelling coupled geomechanical and hydrological behaviour of fractured rocks. *Computers and Geotechnics*, 85:151–176.

Liu, X., Zhang, C., a. Q., and Birkholzer, J. (2008). Multiple-point statistical prediction on fracture networks at yucca mountain. *Environmental Earth Sciences*, 57:1361–1370.

Lo, K. (2019). Discrete fracture network modelling in the geneva basin (lower cretaceous carbonates): Implication for geothermal exploration. *Master Thesis*, 1:123.

Lonergan, L., Jolly, R., Rawnsley, K., and Sanderson, D. (2007). *Fractured Reservoirs*. The Geological Society of London, London, England.

Long, J., Aydin, A., Brown, S., Einstein, H. H., Hestir, H., Hsieh, P. A., Nolte, K. g., and Norton (1996). *Rock Fractures and Fluid Flow: Contemporary Understanding and Applications*. The National Academies Press, Washington D.C., USA.

Maerten, L., Maerten, F., Lejri, M., , and Gillespie, P. (2016). Geomechanical paleostress inversion using fracture data. *Journal of structural Geology*, 89:197–213.

Mignan, A., Landtwing, D., Kästli, P., Mena, B., and Wiemer, S. (2015). Induced seismicity risk analysis of the 2006 basel, switzerland, enhanced geothermal system project: influence of uncertainties on risk mitigation. *Geothermics*, 53:133–146.

Min, K.-B. and Kim, H. (2012). In-situ stress estimation in geothermal reservoirs. *Destress*, 10:1–3.

Moeck, I., Kwiatek, G., and Zimmermann, G. (2009). Slip tendency analysis, fault reactivation potential and induced seismicity in a deep geothermal reservoir. *Journal of Structural Geology*, 31:1174–1182.

Moscariello, A. (2019). Exploring for geo-energy resources in the geneva basin (western switzerland): opportunities and challenges. *Swiss Bulletin für angewandte Geologie*, 25:105–124.

Moscariello, A. (2021). Landscapes and landforms of switzerland: The geomorphological landscapes in the geneva basin. *World Geomorphological Landscapes: Springer Nature Switzerland*, 1:83–96.

Moscariello, A., Do Couto, D., and Omodeo Salé, S. (2020a). An analysis of the petroleum system in the swiss molasse basin with a focus on western switzerland (uncongas). *Rep Swiss geol. Surv.*, 100:1.

Moscariello, A., Guglielmetti, L., Omodeo Sale, S., De Haller, A., Eruteya, O., Lo, H. Y., Clerc, N., Makhloufi, Y., Do Couto, D., , Oliveira, F. D., G., Perozzi, L., De Oliveira Filho, F., Hollmuller, P., , Quiquerez, L., Nawratil De Bono, C. F., Martin, F., and Meyer, M. (2020b). Heat production and storage in western switzerland: advances and challenges of intense multidisciplinary geothermal exploration activities, an 8 years progress report. *In Proceedings World Geothermal Congress*, 1:112.

Niven, E. and Deutsch, C. (2010). Relating different measures of fracture intensity. *CCG Annual Report*, 12:103–107.

Notre Dame, U. (2020). Rock mechanics - response of rocks to applied loads https://www3.nd.edu/ cneal/planetearth/chapt-11a-rock-mechanics.pdf.

O'Brien, J. and Hodgins, J. (1999). Proceedings of the 26th annual conference on computer graphics and interactive techniques. *VU Center and College of Computing*, 26:137–146.

Perozzi, L., Guglielmetti, L., and Moscariello, A. (2020). Geothermal reservoir characterization using seismic and machine learning - a case study from the geneva basin. *Proceedings World Geothermal Congress 2020*, 1:1–8.

Radwan, A. and Sen, S. (2021). Characterization of in-situ stresses and its implications for production and reservoir stability in the depleted el morgan hydrocarbon field, gulf of suez rift basin, egypt. *Journal of Structural Geology*, 148:0–18.

Richter, A. (2020). Switzerland continues its bet on geothermal energy. *Think Geoenergy*, 1:1.

Rountree, C. L., Kalia, R., and Lidorikis, E. (2002). Atomistic aspects of crack propagation in brittle materials: Multimillion atom molecular dynamics simulations. *Annual Review of Material Research*, 12:377–400.

Rountree, C. L., Kalia, R., Lidorikis, E., S. M., Javadi, M., and Zarei, H. (2012). The role of geological structures to tunnel inflow, modelling strategies and predictions. in: Phienwej, n., boonyatee, t., (eds): Tunnelling and underground space for a global society: Proceedings of the ita-aites. *World Tunnel Congress*, pages 377–400.

Shackleton, J., Cooke, M., and Sussman, A. (2005). Evidence for temporally changing mechanical stratigraphy and effects on joint-network architecture. *Geology*, 33:101–104.

Shapiro, S. (2015). *Fluid Induced Seismicity*. Cambridge University Press, Berlin, Germany.

Shlyannikov, V., Martínez-Pañeda, E., Tumanov, A., and Khamidullin, R. (2021). Mode i and mode ii stress intensity factors and dislocation density behaviour in strain gradient plasticity. *Theoretical and Applied Fracture Mechanics*, 116:1–26.

Sommaruga, A., Mosar, J., Schori, M., and Gruber, M. (2006). Post-variscan (end carboniferous – early permian) basin evolution in western and central europe. *Geological Society London Memoirs*, 31:355–388.

Stead, D., Wolter, A., and Clague, J. (2015). A critical review of rock slope failure mechanisms: the importance of structural geology. *Journal of Structural Geology*, 74:1–23.

Trifu, C. (2002). *The Mechanisms of Induced Seismicity*. Birkhauser Basel, Ontario, Canada.

Underwood, C., Cooke., M., Simo, J., and Muldoon, C. (2003). Characteristics of joint propagation across layer interfaces in sedimentary rocks. *American Association of Petroleum Geologists Bulletin*, 87:121–142.

Voigt, M. (1966). *Lehrbuch der Kristallphysik Teubner*. Teubner, Leipzig, Germany.

Vuataz, F. and Fehr, A. (2000). 25 ans d'activite geothermique en suisse. *Geothermie CH*, 26:1–154.

W.A., L. and Pascher, C. (1996). *Induced Seismic Events*. Birkhauser Basel, Teltow, Germany.

Walch, A., Mohajeri, N., Gudmundsson, A., and Jean-Louis, S. (2021). Quantifying the technical geothermal potential from shallow borehole heat exchangers at regional scale. *Renewable Energy*, 165:369–380.

Welch, M. J., Lüthje, M., and Oldfield, S. J. (2022). Dfn generator v2.0: A new tool to model the growth of large-scale natural fracture networks using fundamental geomechanics. *Geosci. Model Dev. Discuss*, 22:42.

WellCAD (2021). *WellCAD: https://www.alt.lu/products-wellcad/*. Advanced Logic Technology, Redange, Louxembourg.

Welsch, M., Luthje, M., and Oldfield, S. (2020). *Modelling the Evolution of Natural Fracture Networks*. Springer, Switzerland.

Wiprut, D. and Zoback, M. (2000). Fault reactivation and fluid flow along a previously dormant normal fault in the northern north sea. *Geology*, 28:5965–5981.

Wyering, L., Villeneuve, M., Kennedy, B., Gravley, D., and Siratovich, P. (2017). Using drilling and geological parameters to estimate rock strength in hydrothermally altered rock – a comparison of mechanical specific energy, r/n-w/d chart and alteration strength index. *Geothermics*, 69:119–131.

Wyss, R. and Rybach, L. (2010). Developing deep geothermal resources in switzerland. *World Geothermal Congress 2010*, 1:1–4.

Xu, C., Dong, S., Wang, H., Wang, Z., Xiong, F., Jiang, Q., Zeng, L., Faulkner, L., Tian, Z., and Dowd, P. (2021). Modelling of coupled hydro-thermo-chemical fluid flow through rock fracture networks and its applications. *Geosciences*, 11:227–236.

Xueliang, X., Shunchuan, W., Aibing, J., and G, Y. (2018). Review of the relationships between crack initiation stress, mode i fracture toughness and tensile strength of geo-materials. *International Journal of Geomechanics*, 18:1–20.

Zhang, L.-M., Qi, J., Zhang, K., Li, L.-X., Zhang, X.-M., Wu, H.-Y., Chipecane, M. T., and Yao, J. (2019). Calibrate complex fracture model for subsurface flow based on bayesian formulation. *Petroleum Science*, 16:1105–1120.

Zoback, M. and Kohil, A. (2019). *Unconventional Reservoir Geomechanics: Shale Gas, Tight Oil, and Induced Seismicity*. Cambridge University Press, New York, USA.

A | LITHOLOGICAL DESCRIPTION

Top [m] MD	Lithological Description
410.8	Bioclastic limestones, white to light beige, highly recrystallized, frequent pyrite
414	Bioclastic to oolitic limestones, light beige to white, very recrystallized, leaving totally bronze, calcite veins
418	Light beige to white bioclastic to oolitic limestones
420	Yellowish limestone with ooids and bioclasts
422.5	Peloidal bioclastic limestones, fine to medium, slightly oolitic, yellow to orangeish, finely sandstone, with pyrite and glauconite
426.5	Sandstone, pyritic and glauconious, grey-green and gray bioclastic limestones and some sandstone-glauconicious marls. Cuttings coming out completely crushed between 430 and 432 m
432	Bioclastic sandstone, pyritic and glauconious limestone, grey-green and grey, numerous veins of white calcite with passages of gray and reddish sandstone-glauconitic marl
449	Sandstone, glauconious and pyritic marls, dark grey, presence of red and ocher clay at 455m
456	Alternating sandy, glauconious and pyritic marls, dark gray and softer sandy marls, light gray
458	Fine limestone, grey-green, sandstone-pyrito-glauconitic and some light gray soft sandstone marls
460	Alternation of fine gray-green marly limestone, sandstone-pyrito-glauconitic, dark gray sandstone clacareous marls, presence of red and ocher clays (fracture filling?) Interval with cuttings silt size
475	Glauconious bioclastic limestones, gray to greenish gray
476	Biodetritic sandstone-glauconitic marly limestones, greenish to gray and dark gray to black calcareous marls
480	Light gray to slightly dark gray sandstone-glaucous shale marls
495	Sandstone marls to glauconious, gray marly sandstone, and a few passages of sandstone-glaucous, greenish-grey bioclastic shale
512	Greso-glauconious, greenish-gray marly limestone
513	Yellowish bioclastic limestones, strongly recrystallized, with some yellow oolites and bryozoan debris. Numerous flakes of white calcite from 516 to 520 m (fractures)
516	Yellowish oolitic limestone rich in pyrite. Fractures/fissures at 518-519 m
522	Alternation of yellowish oolitic limestones rich in pyrite (red limestone facies) and white-grey oobioclastic limestones (grainstone - Chambotte facies inf.?) Fractured zone
526	Yellowish-white to gray oo-bioclastic limestones (red limestone facies). Presence of fractures

B FRACTURE PICKING

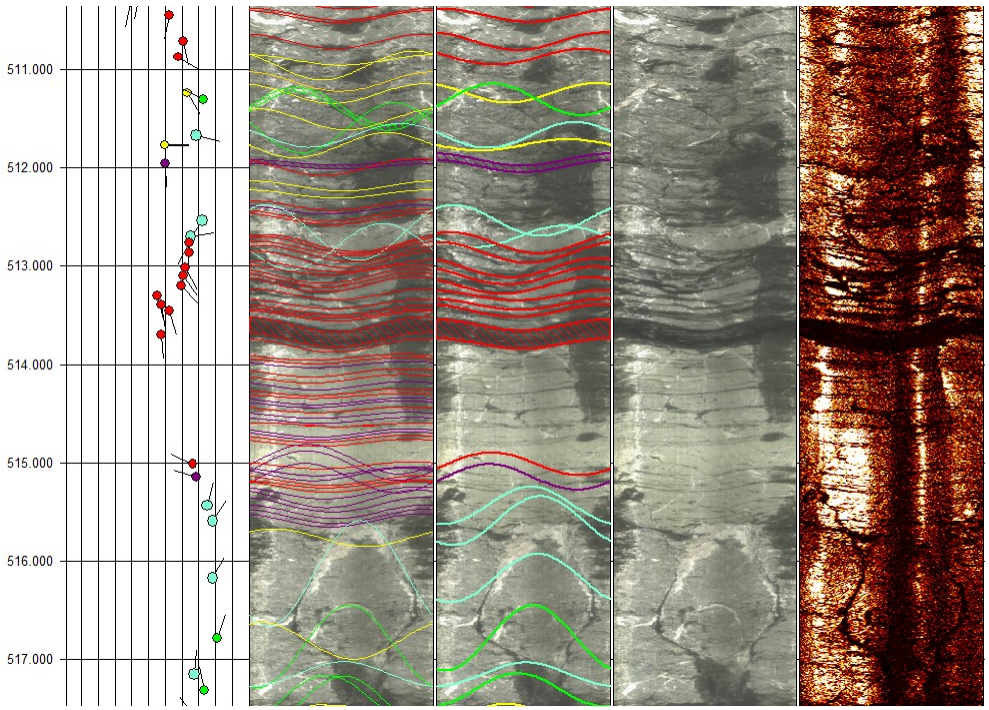

Figure B.1: WellCAD fracture picking

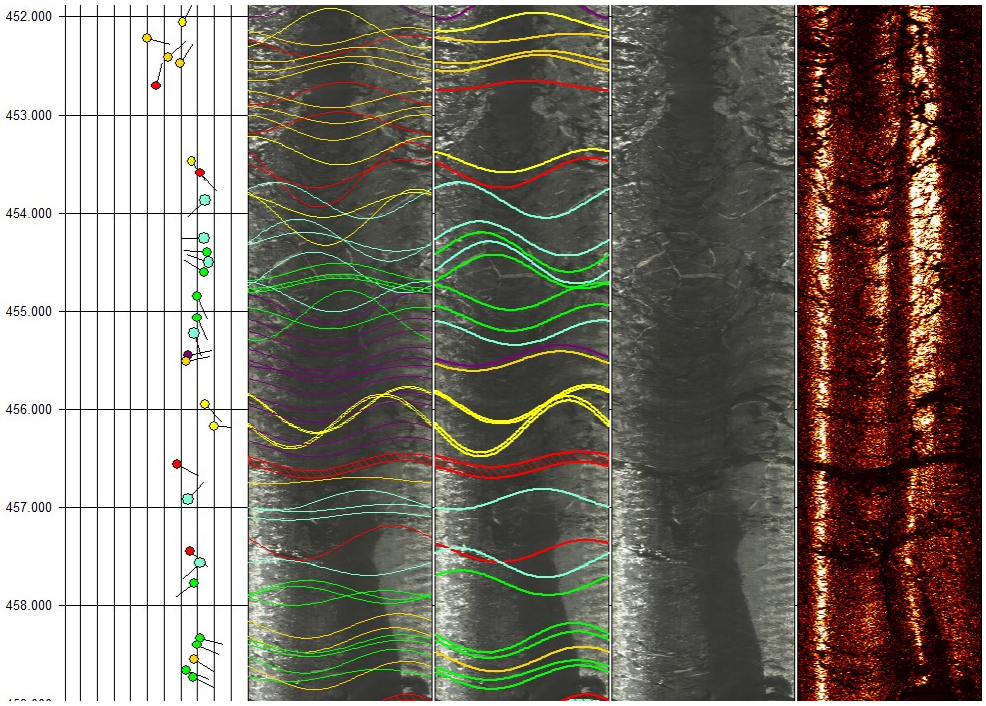

Figure B.2: WellCAD fracture picking

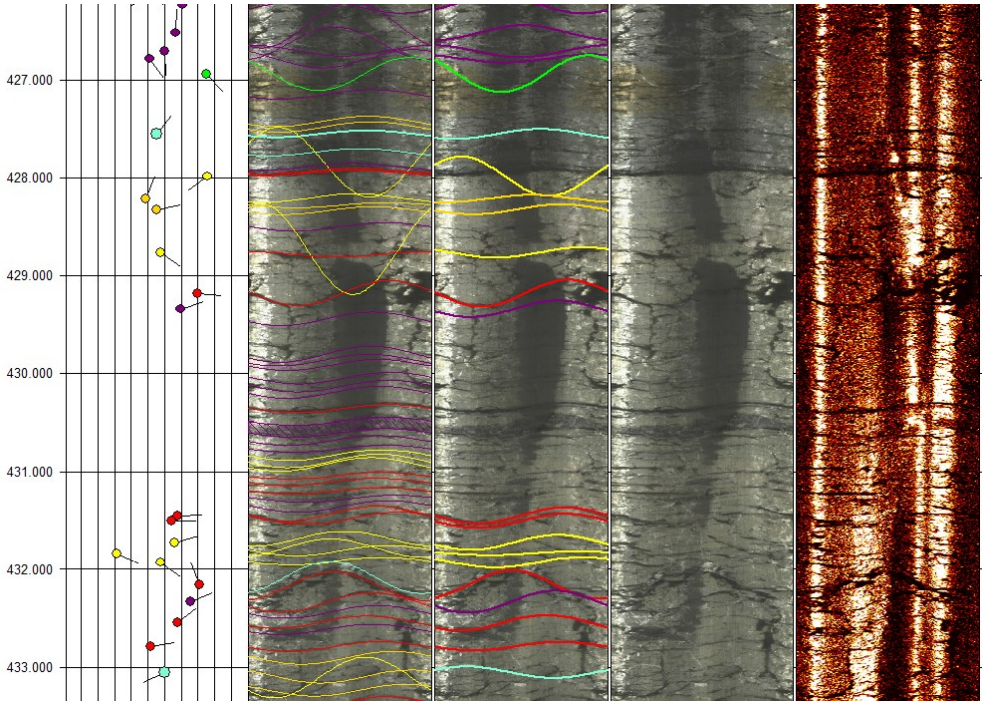

Figure B.3: WellCAD fracture picking

C PALEO-TECTONIC STRESS

The graph in Figure C.1 shows that there is a high probability within σH orientations between 30 and 110 degrees the faulting regimes has a probability of 0.5. While a strike slip regime has a probability of 0.55 with σH values between 110 and 160.

In sub figure 'e' for the Marnes d'Hauterive formation the graph is showing that there is a high probability that the stress regime in that area is a strike slip stress regime with a σH orientation of roughly 140 degrees. The graph is also showing that there is a very low probability that the σH is oriented in the 90 to 20 degrees. From these graphs, the values of the stress in bar are also calculated. These values turned out to be very low to a magnitude of E-6bar. In some cases the σV values turned out to be zero which is very likely not the case.

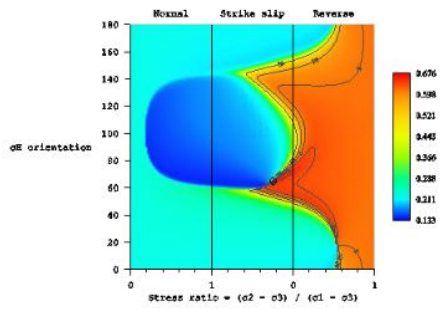

(a) Urgonien blanc et jaune - Scenario 1

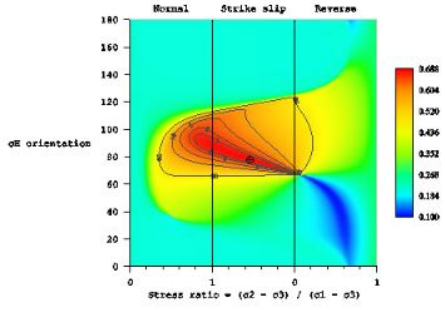

(b) Urgonien blanc et jaune - Scenario 2

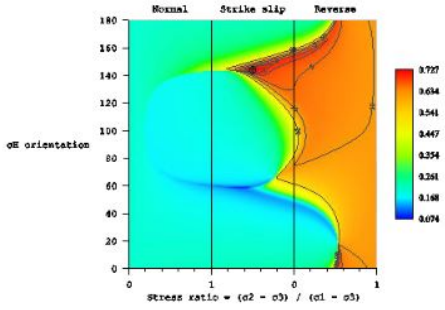

(c) Pierre Jaune de Neuchatel- Scenario 1

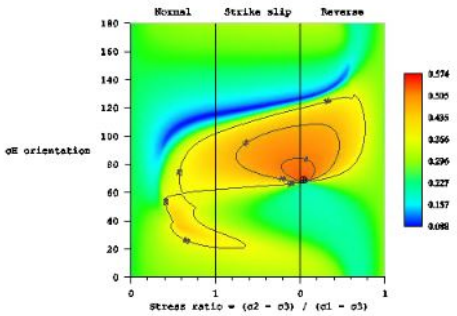

(d) Pierre Jaune de Neuchatel- Scenario 2

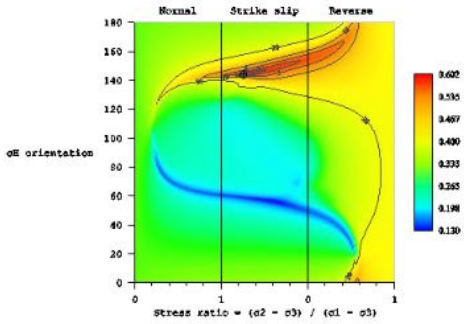

(e) Marnes d'Hauterive- Scenario 1

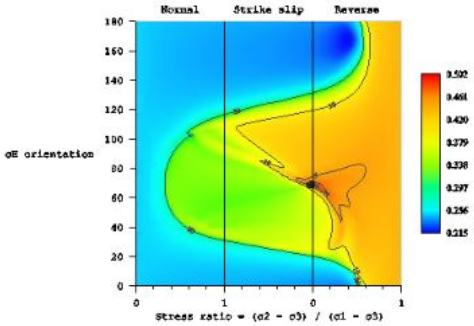

(f) Marnes d'Hauterive- Scenario 2

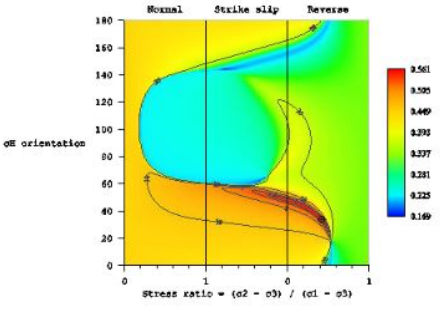

(e) Complexe.. Scenario 1

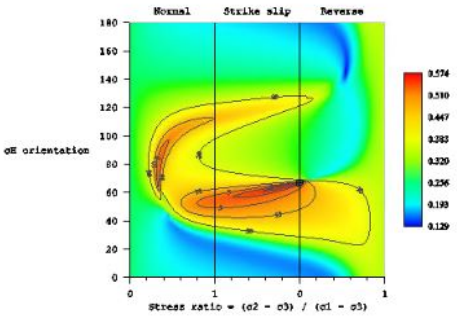

(f) Complexe.. Scenario 2

Figure C.1: Paleo-Stress inversion calculation through petrel

COLOPHON

This document was typeset using LaTeX. The document layout was generated using the arsclassica package by Lorenzo Pantieri, which is an adaption of the original classicthesis package from André Miede.